University of Genova

Ph.D. Program in Neuroscience

The role of Piezo1 in an *in-vitro* neuron-like system

Candidate

Martina Zambito

Supervisor

Prof. Tullio Florio

XXXIV cycle 2018-2021

ABSTRACT

Cells undergo an enormous amount of mechanical stimuli from extracellular matrix and surrounding cells and tissues. These stimuli have been underestimated for years, but recently, several studies highlighted their importance in physiology and diseases. Indeed, many pathological conditions contribute to create peculiar environments that lead to biomechanical abnormalities, as occurs in tumors or in neurodegenerative diseases. Piezo1 is a mechanosensitive calcium-permeable ion channel. Its expression is involved in the maintenance of cerebral homeostasis, making it a relevant potential pharmacological target in different pathologies. This project aims to outline the role of Piezo1 channel in mouse immortalized mesencephalic neuron-derived cell line (A1) by its overexpression (A1-OV) and pharmacological modulation, in different stiffness culture settings. *In-vivo*, cell environment displays lower elasticity (0.2-64 kPa) as compared to the common *in-vitro* culture ($1x10^7$kPa). We evaluated how cells change and adapt to a different stiffness substrate, analysing shape, elasticity, gene expression, viability, and functional activity. A collateral part of this work was dedicated to the characterization of the nanoindentation technique through the Chiaro nanoindenter, in order to find a correct methodological approach to measure cellular elasticity. A1 cell viability is stiffness-dependent, directly paralleling substrate stiffness. WT A1 cells plated in softer substrate and A1-OV in plasticware change their shape modifying the expression of cytoskeleton components. Notwithstanding in these experimental conditions cells are characterized by higher basal concentration calcium ions, they also display an increased response to the Piezo1 agonist Yoda1 in terms of Ca2+ entry. Furthermore, we assessed the capacity of Amyloid-beta to affect the mechanical property of A1 cells. The non-aggregated “monomeric” peptide-induced cell stiffening, while aggregated Amyloid-beta caused cell softening. Further experiments will be required to confirm these data and correlate them with cell functional changes. Altogether, the data here reported show that neuron-like cells adapt in different stiffness settings changing their characteristics according to the biomechanical features of the substrate in which they are plated or in response to molecular treatment. These changes could, at least partially, involve Piezo1, making it an interesting pharmacological target.

Contents

1. INTRODUCTION

David Julius and Ardem Patapoutian received the last Nobel Prize in Physiology or Medicine (2021) for their studies on thermal and mechanical transducers. All living beings are sensory beings. Animals, like us, are covered with sensors in every single part of their body. In the beginning, because perception passed through the nervous system, the sensation was related to neuronal transmission, and sensory neurons have been deeply studied. However, the sensation is covered by different kinds of stimuli like vibration, pain, pressure, heat, among others, which can be perceived by cells through dedicated channels.

The importance of this kind of transducers is nowadays emphasized thanks to researchers like Julius and Patapoutian.

1.1 MECHANOSENSITIVE ION CHANNELS

Mechanosensitive channels (MSCs) encompass a family of channels able to sense all kinds of mechanical force around them. In the seventies of the twentieth century, the first evidence about their existence was discovered in prokaryotes after a mechanical stimulation in the inner ear hair cells [1]. It was discovered that, after stimulation, MSC forms the membrane pore and conducts ions in a non-selective way. Two different kinds of channels were distinguished at the beginning in comparison to their composition or structure: MscL (mechanosensitive channel large conductance) and MscS (mechanosensitive channel small conductance). These kinds of channels were found in several species like fungi, bacteria, and animals, suggesting conservation across all organisms.

The activity of MSC is stimulated by external or internal cues. The external cues could be related to external forces or to the substrate to which cells adhere. For the first one, the

more common are shear flow, tension and compression, pressure, poking, stretch, shear stress, and swelling. For the second one the geometry, nano-topography, and the stiffness of the substrate trig the channel activity. The internal cues could be divided among the influence of the extracellular matrix (ECM), the composition and movement of the membrane, and the cytoskeleton contribution. Plasma membranes are not static, but fluid and in continuous movement. When the membrane changes its deformation leads to a mechanical change perceived by MSC. The bilayer could be thinner or bigger depending on the association of lipidic force. Lytic tension leads to the entry of water in the membrane and the consequent separation of lipids leading to a hydrophobic disruption of membrane cohesion. Smaller is the lipid bilayer easier is to bend the membrane[2]. All these characteristics are linked to the sensitive portion of MSC but that must to be converted into electrical or biochemical signals in a mechanism known as mechanotransduction. Some of these putative receptors are presented in *Fig.1* and in particular, our object of study is Piezo1 [3].

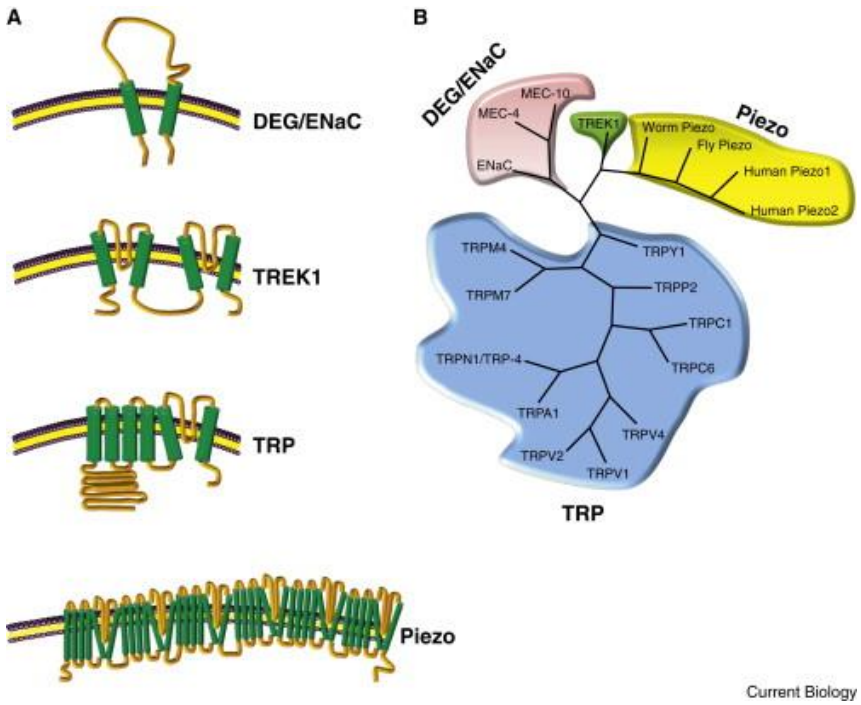

Figure 1 **Mechanosensitive channels in eukaryotes**. Schematic representation of mechanosensitive channels in eukaryotes (A). Dendrogram plot of separate classes of presumed mechanosensitive channels. In TRP family channels, TRPV1 is the only protein that has been demonstrated to function as a mechanosensitive channel (B)[4].

1.2 PIEZO1 CHANNEL

In 2006, under the name of Mib (KIAA0233 in Human) a new membrane protein associated to astrocyte cells was discovered in the amyloid plaque[5]. In January 2010 a new transmembrane domain protein was identified as an activator of integrin-ligand affinity, called Fam38A. The authors showed that R-Ras or calpain are able to block the channel activation causing a reduction in cell adhesion[6]. These two proteins were later associated to a mechanosensitive receptor, discovered in the neuroblastoma cell line (N2A) by Patapoutian et al. [7]. The purpose of this group was to identify proteins involved in mechano-transduction, applying mechanical force with a glass probe, and recording cells through patch-clamp techniques. They found a significant reduction in mechano-activated current after knocking down Fam38 gene, so the protein encoded was named Piezo1 from the Greek word 'píesi' that means pressure. Piezo1, like any other MSC, is permeable for cation K^+, Mg^{2+}, Na^+, with a preference for Ca^{2+} [7]. For these two decades, Piezo1 was studied in different fields and several tissue or pathologies because it was a channel preserved under different species and ubiquitous expressed in cell and tissue.

1.2.1 Structure

Piezo channels compose a family of two different channels with a different activity but basically the same structure. These channels have the largest number of transmembrane domains of all known proteins (42) organized in a homotrimeric structure for a total amount of 900 kilodaltons. Through a combination of live-cell immunostaining, X-ray crystallography and, cryo-electron microscopy, it was evident that its 3D structure resembled a propeller composed of three blades and a central pore[8]. The *Fig.2* reproduces a possible view of the channel, allowing a possible look at the different components. It is composed by intracellular and extracellular parts combined with an enormous amount of transmembrane domains. The extracellular domain is composed of the curved blades, for mechanotransduction, and a cap region composed of the C-terminal extracellular domains (CED). The continuous of the blades are embedded in the membrane where a little portion called anchor, a hairpin structure with a long helix that penetrates inside the membrane in a parallel way. The anchor, necessary for the stabilization of Piezo1

structure, has the most conservative sequence of the channels. Six transmembrane helices from the central pore for conducting ions. Then in the intracellular site, three beams are important for the connection of all the parts of the channel used as a pivot for the blades when mechanical changes occur allowing the opening of the channel and the consequents ions flux [9].

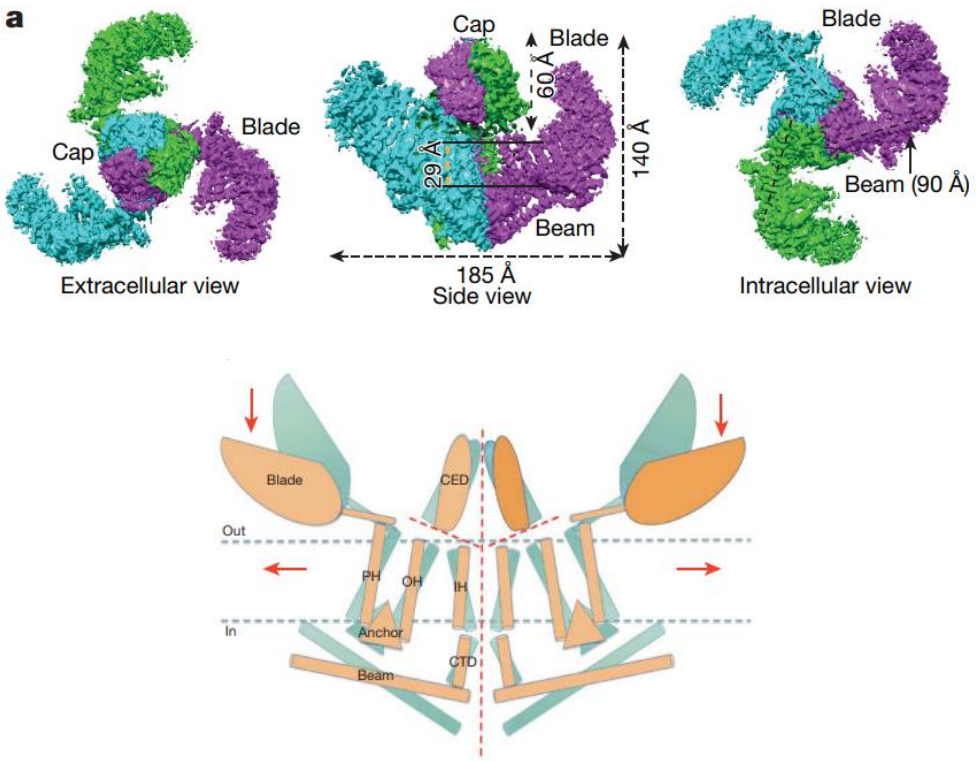

Figure 2 **Piezo1's structure** Top, bottom and side views of a physiological map of Piezo1, with distinct regions and dimensions labelled. Proposed model of the force-induced gating of Piezo channels. The blue and orange models represent the closed and open state channels, respectively. Red dashed lines indicate the possible ion conduction pathways. Presumably, when the blades flatten due to external forces (red arrows) the channel gets open[7].

1.2.2 Pathological and biological implication of Piezo1

A complete depletion or inactivation of Piezo1 in embryonic stages is lethal for several mice models, but the heterozygous mouse is viable with a less vascular organization [10], [11]. Indeed, it was demonstrated that channel expression increases during embryonic stages. This condition underlies the importance of Piezo1 during vasculature development that could be the reason for the lethality when total depletion is induced. In humans, two

pathologies are related to homo- or heterozygosis missense mutation of the channel: the autosomal dominant dehydrated hereditary stomatocytosis (DHSt known as hereditary xerocytosis) and the generalized lymphatic dysplasia (GLD).

In DHSt, mutations alter the activity of Piezo1. It is characterized by rapid opening in response to all the possible mechanical stimuli, with a consequent rapid inactivation (around ten milliseconds) [7]. Some of these mutations affect the current decay and its reduction, so they are considered gain-of-function mutations, underlying the high physiological importance of the inactivation [12]. Increasing cations transport in erythrocytes cause haemolysis, due to a red cell osmotic fragility that also leads to an alteration of erythrocytes' volume regulation, and they look dehydrated [13]. To provide the specific role of Piezo1 erythrocytes treated with Yoda1 displayed the same morphology as DHSt [14].

GLD is a rare disease causing lymphoedema in the whole body. Red cells acquired a different cellular shape named stomatocyste, and are characterized by an initial spherocytosis and a subsequent cation leak [15], [16]. In this case, Piezo1 mutations induce channel loss of function and thus its activity decreases with no calcium flux.

DHS and GLD are the only two human pathologies associated with Piezo1 mutation. However, Piezo1 has been studied in a lot of different mechanosensitive tissue and the results about its implication underlie its important role.

The endothelial cells on the vasculature's walls are subjected to mechanical stimuli like share stress and tensile forces due to blood pressure. It seems that this channel can control blood pressure and later ATP release after its activation. In the same way, Piezo1 might control the microvascular tone and red blood cells' deformation with a controlled release of ATP [17], [18].

During movements, chondrocytes are squeezed by compressive forces and exposed to shear stress from the synovial fluid or tensile force due to the connection with the surrounding matrix. In this tissue, the pharmacological reduction of Piezo1 activity suggests

a decrease of cells death after a mechanical injury that seems linked to the increase of [iCa^{2+}] in chondrocytes after high forces [19].

In lung cells, Piezo1 expression supports the activation of integrin signalling cascade. Silencing or depleting the channel causes a reduction in cells adhesion and the promotion of migration that could be enforced lung cancer phenotype[6],[20]. These traits are common in cancer cells. So, in recent years, several studies underlie the importance of biomechanics in tumors. It was demonstrated that cancer cells in the inner masses are softer than other cells, facilitating cell division. On the other hand, cancer cells are surrounded with a stiffer extracellular matrix that can activate invasiveness mediating mechanisms. Both conditions promote tumors progression and malignancy [21]. Thus Piezo1 could represent a biomarker in tumors, and its possible modulation could be fundamental to mitigate cancer aggressiveness.

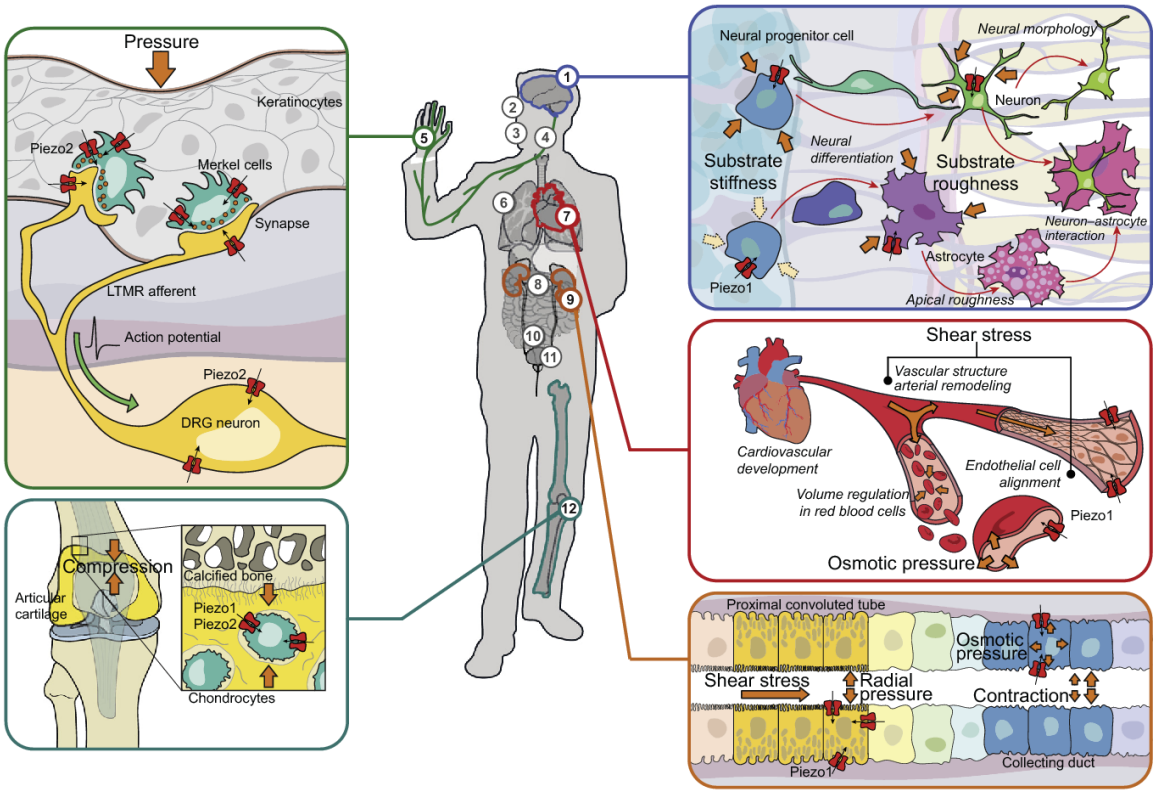

Figure 3 **Roles of Piezos**. Piezo1 and Piezo2 are expressed in a diverse set of cells and tissues within the human body, contributing to an equally diverse set of physiological roles[22].

Xin Chen et al. have demonstrated the role of mechanics and Piezo1 channel in the progression of a still incurable tumor, the glioblastoma, the most common malignant brain tumor. They proposed a feedforward circuit in which the abnormal mechanics of the tissue

and the mechanotransduction in tumor cells promote malignancy[23]. They suggest that with the increasing of ECM stiffness, the activity of Piezo1 increases promoting the positive feedback of the expression of genes involved in ECM remodelling. On the other hand, the increase in Piezo1 activity leads to an upregulation of Piezo1 expression.

1.2.3 Possible interactors or channel opening modulators

How Piezo1 convert all the mechanical stimuli into biological signal is not yet completely known, but some possible interactors were identified.

The Sarco- endoplasmic reticulum Ca^{2+} ATPase (SERCA) transports Ca^{2+} from the cytoplasm to the sarcoplasmic or endoplasmic reticulum (SR/ER). It was demonstrated that this transporter not only physically interacts with Piezo1, but it acts as a suppressor of its activity. The anchor region of Piezo1 (previously described) is the focal point of interaction with Piezo1 and SERCA2A, when its sequencing changes, they do not pull down together during an immunoprecipitation, but you can distinguish two single bands in a western blot analysis. This interaction affects Piezo1 activity by the reduction of poking/stretch-induced current, reduction in eNOS phosphorylation, consequent cell migration, and then the increase in its inactivation rate [24].

The stomaton-like protein3 (STOLM3), the unique member of its family is able to facilitate the mechano-sensibility of Piezo1 and it is also fundamental for several mechanosensitive channels in sensory neurons [25], [26]. Touch receptors in mice need a displacement threshold around 13nm for being activated. STOLM3 reduces the threshold activation for Piezo1 under 10nm, and its depletion increases this parameter of one order of magnitude. It is a protein linked to the membrane and usually is associated to lipid raft where cholesterol is one of the main components. Membrane's stiffness changes after reduction of cholesterol in lipid raft, or STOLM3 depletion in neurons, causing modifications of the stiffness of the membrane, and altering the sensibility of the channel [27]. For the same reason, the activation of TRPV1 (transient receptor potential cation channel subfamily V member 1) channel leads to inhibition of Piezo1 due to the consequent activation of phospholipase C (PLC), causing hydrolyzation of membrane phospholipids like PIP and PIP2 [28]. Each phosphoinositide is required to maintain Piezo1 currents.

It has also been observed that cytoskeletal protein can modulate Piezo1 activity. In particular, in smooth muscles cells, filamin A (FlnA) repressed the opening of Piezo1. In absence of FlnA cytoskeleton's structure got destroyed and cells become softer, resulting in an increase in membrane tension that alters the opening of the channels [29]. These results and others strengthen the importance of membrane structure changes as mechanisms that alter Piezo1 activity.

1.2.4 Pharmacological modulation

In light of all the possible implications of Piezo1 in physiological and pathological processes previously described, the pharmacological modulation of its activity becomes a relevant clinical issue. The first channel blocker used, has been the neurotoxin GsMTx4, which, however, is not selective for Piezo1, but can inhibit also other MSCs. It is a small peptide of 4kDa isolated from the venomous tarantula, *Grammostola spatulate* [30]. It inhibits target channels acting like a gating modifier and not as a pore blocker, because of its amphipathic nature that allows GsMTx4 to interact with the cell membrane. Indeed, it is not specific for any portion of MSCs but acts through the binding to lipidic bilayers influencing the mechanical property of the membrane. GsMTx4 can also form dimers when one of its molecules is just linked to the bilayer [31]. Through this mechanism, this neurotoxin seems to have a double effect on two channels at the same time, Piezo1, and TREK. The tension change in the outer monolayer of the membrane, after GsMTx4 interaction, and it is transferred to the inner monolayers increasing the tension to this side that cause TREK activation [32]. A stronger mechanical stimulus can reverse the effect of GsMTx4 which confirms its mechanism of action as a gating modifier instead of a pore blocker. Other possible blockers used in studying MSCs activity are ruthenium red, streptomycin, and gadolinium.

On the other hand, no existing molecule can be used to evoke the activity of Piezo1. So, in 2015, Syeda et al. synthesized a compound with a low molecular weight named Yoda1 [33]. It is very efficient at micromolar concentrations and acts stabilising the open state of the channel with a consequent reduction of the mechanical threshold for its activation, and inactivation kinetics. Yoda1 binds a specific region of each blade's subunits and exerts its activity both from the inner and the outer side of the membrane. Remarkably, it does not

affect Piezo2. Most recently was synthesized an analogue of Yoda1 termed Dooku1, which is able to reversibly antagonize Yoda1-induced activation of Piezo1 by competing for a specific channel binding site [34].

Through high-throughput screening assays, other chemical activators have been created, named Jedi1, and Jedi2. These molecules share a 3-carboxylic acid methyl-furan motif, implicated in the activation of Piezo1 only in the extracellular side of the blades [35].

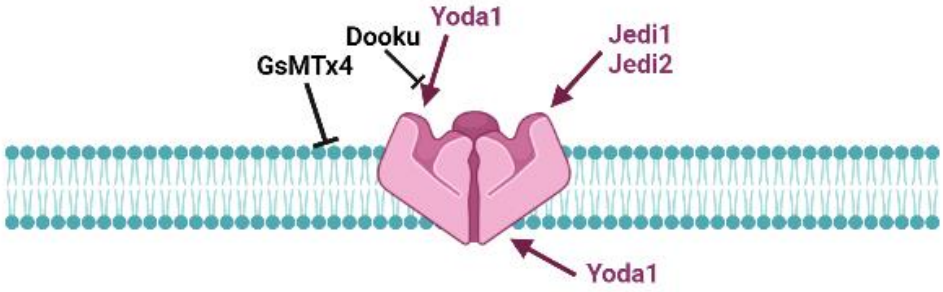

Figure 4 **Chemical compounds** Schematic picture of all known chemical interactors of Piezo1 (from Biorender)

1.3 Mechanobiology

Mechanobiology represents the study of all possible factors playing a role in physical or biomechanical changes that contribute to differentiation, growth, motility, and adhesion in cells and tissues. It is a field that has attracted different specialized figures. Biologists, engineers, chemists, and physicists have had to interact. The just described mechanoreceptor Piezo1 is an important player in this pathway, as well as other MSCs. But to better describe all these processes, we need to introduce additional actors. One of them is the cytoskeleton and its organization. It is non-static but in continuous rearrangement. Its changes are perceived and transduced by mechanoreceptors, or in the other way, channel activity could modify the cytoskeleton organization.

The cytoskeleton is composed of three main components: actin filaments, intermediate filaments, and microtubules. Microtubules provide the basic organization of the cytoplasm. Through polymerization and depolymerization, they grow and change dynamically. Their biomechanical properties are resisted compressive forces [36]. Actin filaments are the main

structural components of the cytoskeleton and respond to external forces through deformation and rearrangement. Actin filaments make the cell cortex, which is a specialized layer on the inner face of the cell membrane, responsible for the modulation of membrane properties and more generally of cell surface properties. The integrin-based adhesion complexes are closely associated with the actin cytoskeleton and are able to recognize not only the biochemical molecules of the extracellular surroundings but also their physical and geometrical characteristics such as elasticity, dimensionality, and ligand spacing. The extracellular matrix (ECM) is another important component in mechanobiology, it gives physical support to the cells. It composes the external environment of the cells [37].

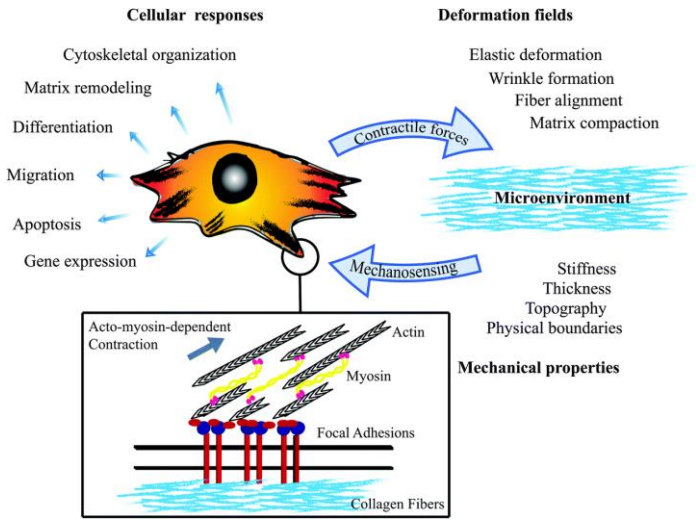

Figure 5 **Mechanobiology** Illustrative cartoon of cellular and extracellular response to mechanical stimuli[38].

It has been demonstrated that changing the substrate where the cells are seeded, alters their gene expression in pathway that leads to a cell lineage specification, as demonstrated in adult stem cells. This lineage is able to engraft and differentiate in all tissues. Each tissue is characterized by a specific matrix microenvironment that can be extremely different considering tissues like brain and osteoid. Engler et al. demonstrated that adult stem cells can modulate gene expression, choosing a specific lineage in which differentiate, only providing the support of different substrates on which cells are plated (*Fig.6*) [39].

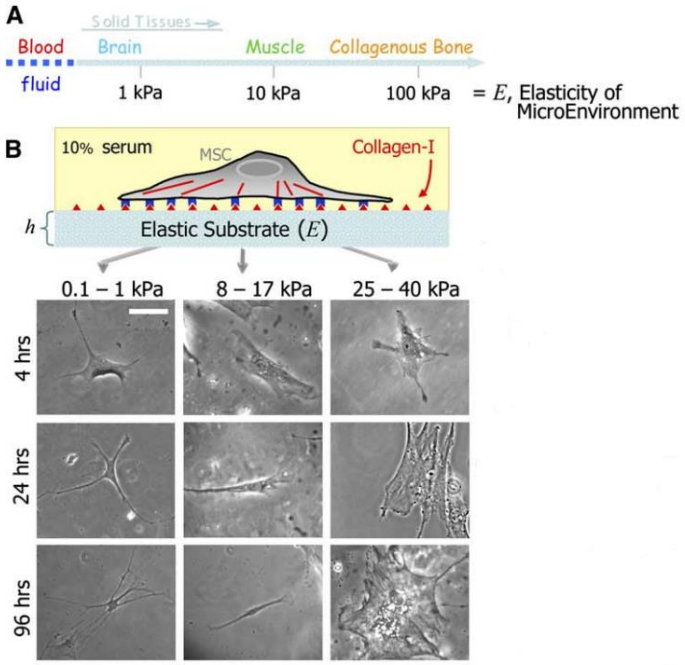

Figure 6 **Matrix elasticity directs stem cell lineage specification**[39]

Other important players are transcriptional factors. Indeed, when something in a cell changes there will be upstream or downstream (or both) genetic regulations. Through bioinformatic analysis, performed in mammary epithelial cells (MEC) grown on ECM from high versus low stiffness, were identified differentially expressed genes. So, in 2011 YAP/TAZ have been found as transcriptional molecules upregulated when MEC has grown in an ECM with high stiffness. It was also demonstrated that cells on soft matrices (in the range of 0.7–1 kPa) inhibited YAP/TAZ expression to levels comparable to siRNA- YAP/TAZ [40]. More in detail, Yap and Taz localize within the nucleus on stiff substrates, but on soft substrates, they are shuttled to the cytoplasm. It was demonstrated that, in human neural stem cells, Piezo1 knockdown can reverse the mechanical cue for localizing Yap to the nucleus, highlighting that Yap could be a downstream effector of Piezo1 activity [41].

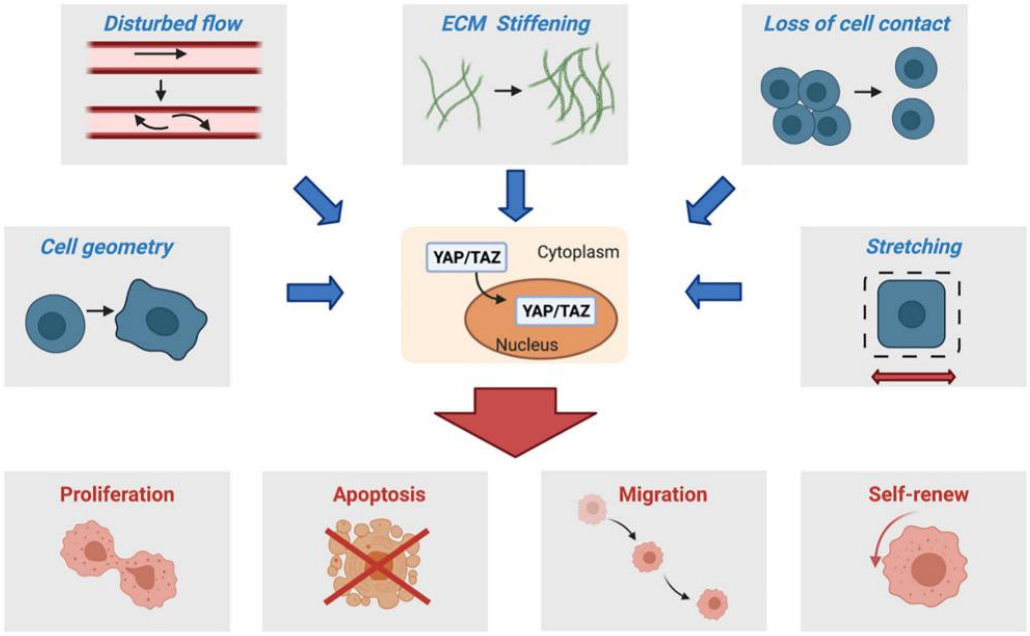

Figure 7 **Cause and effect of nuclear translocation of Yap/Taz** Mechanical impairs promotes nuclear translocation of Yap/Taz and this leads to transcriptional activation of genes involved in cell proliferation, apoptosis, migration, and self-renew[42].

1.3.1 Techniques for cell mechanics studies

Techniques to study cell mechanics can be categorized in terms of their application in cell mechanics and cell-ECM interactions. Some limitations of these kinds of techniques are related to the low throughput and the direct contact to the cell that may cause cellular responses. We can include AFM-based methods, magnetic twisting cytometry, and cytoindentation to exert cells' local forces. Single-cell-based techniques are microplate stretcher and micropipette aspiration. Optical tweezers and optical stretchers deform cells without contact. Cell traction force is important for mechanical signal transmission and cell migration and it's the measure of how the cells/cytoskeleton are strong. Cells are plated in particular array with micropillar and are measured their capacity to move these pillars. Most of the techniques are depicted in *Fig 8*.

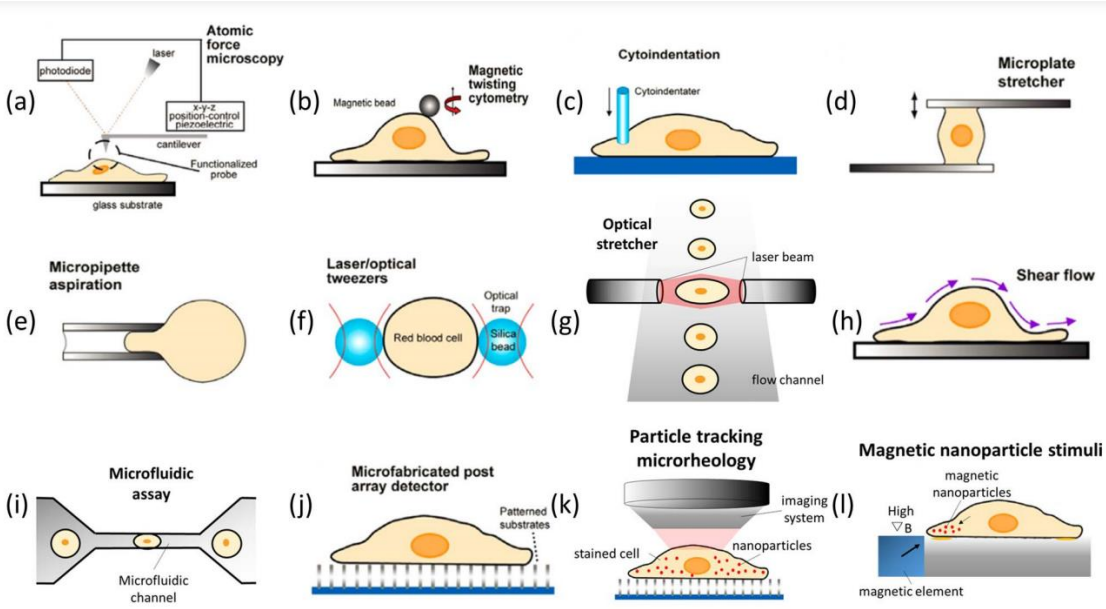

Figure 8 **Major techniques for cell mechanics' study** [43]

1.3.2 Mechano-sensation in brain

The brain is the softest tissue of the whole body, ranging from 0.1 to 1 kPa. It is an isolated organ, protected by the skull and the cerebrospinal fluid. But, despite that, it receives mechanical stimuli from inside that must be converted in biological signals. For many years, neurons were considered as the main actors of sensory transmission. Indeed, electrical aspects of neurons were deeply investigated as biochemical and genetics studies. However, the action potential has an electrical, biochemical, and biomechanical relevance inside cells. It leads to membrane deformation that influences axons and synapsis with a consequent cytoskeleton reorganization [44], [45].

It is known that brain expresses a variety of MSCs, and mutation or dysfunction of such channels can lead to several pathologies. TRPV4 is the most studied due to its high expression in the DRG neurons and astrocytes. Some TRPV4 mutations are involved in the Charcot-Marie-Tooth disease 2C (CMT2C), an autosomal dominant disease characterized by limb, and laryngeal muscle weakness [46]. Recently was also displayed the critical role that Piezo1 plays in neurons and glial cells.

It is known that different pathologies contribute to modifying extra- and intracellular environment that leads to biomechanical abnormalities, as it occurs in tumors or neurodegenerative diseases. Abnormal stiffness actively contributes to disease progression. Changes in the brain stiffness and mechanical properties of the matrix have been associated with different neuropathological conditions, including Alzheimer's disease (AD). Despite AD is a long-time studied disease, and much information was added during the years, not much progress was achieved for its treatment. Several missing pieces have not yet been found so much more research has to be done. Alzheimer's is characterized by an abnormal accumulation of amyloid-beta protein, neurofibrillary tangles, extensive neuronal loss, and Ca^{2+} dysregulation [47]. The accumulation of amyloid beta-protein is one of the most studied mechanisms of neurodegeneration. It originates from Amyloid Precursor Protein (APP), a membrane-bound protein that is sequentially cleaved, producing extracellular Aβ. The cleavage produces different forms of Aβ, such as $A\beta_{40}$ and $A\beta_{42}$. The last one is more commonly associated to pathogenic lesions because can create amyloid oligomers and insoluble fibrils with higher efficiency. Abnormal Aβ accumulation leads to the formation of Aβ plaques that change brain homeostasis and brain stiffness, with the pathological brain resulting softer than the healthy one [48]. Calcium signalling is an important second messenger involved in a multitude of cellular functions, including migration, transcription, apoptosis, secretion, excitability, exocytosis, and neurotransmission. Ca^{2+} entry in cytosol is strictly regulated and maintained at low concentrations by pumps, buffers, and transport mechanisms. Ca^{2+} dysregulation is important in AD.

The first discovered protein Mib, later associated to Piezo1, was found to be expressed in astrocytes associated with amyloid plaques. Normal astrocytes usually do not express Piezo1 but in an inflammatory condition like in the plaques, they upregulate the expression of the channel. In contrast neurons around the lesion down-regulate Mib expression [5]. Years later from the original observation about this pathway, a central role was also given to microglial cells as a possible regulator of Piezo1 expression in astrocytes [49].

It was also discovered the relevance that amyloid-beta peptides have as membrane modifiers. First of all, in 2015 using AFM techniques the change in elasticity in young versus aged neurons, treated with Aβ peptides, was studied. The Aβ molecules affect and change

the mechanical properties of both these cell populations, but aged cells are more susceptible because of the higher affinity of Aβ [50]. The incorporation of Aβ peptides within membranes affects the mechanical properties of lipids, thickness, and decreases the bending rigidity of the membrane [51]. This suggests that membrane's mechanical properties could play an important role in neurodegenerative disorders.

2. AIMS

The aim of the project is to explore the role of Piezo1 channel in mouse embryonic mesencephalic neuron-derived cell line (A1). Piezo1 expression in neurons could be involved in brain's homeostasis and environmental changes during aging, injuries, and neurodegenerative diseases; these reasons make it an interesting object of study. The purpose of this study is to characterize the mechanisms by which different mechanical cues interfere with Piezo1 functioning to modulate neuronal activity and infer whether modification of channel expression may lead to changes in the biomechanics of the cells.

3. MATERIALS AND METHODS

3.1 Cell cultures

A1 cell line was obtained by retroviral infection with immortalizing c-myc gene of mouse embryonic mesencephalic neurons; cells were cultured in DMEM/F12 (Euroclone) with 10% fetal bovine serum (FBS)(Gibco). A1 were differentiated at 50% confluence as reported by Colucci et al. [52] without FBS but with 1Mm N^6, 2'-O-Dibutyryladenosine 3', 5'-cyclic monophosphate sodium salt (cAMP) (Sigma) and N-2 Supplement (100X) (Gibco) (1:100 dilution) up to 6 days. Cells were transfected with human-Piezo1-GFP plasmid (received from Victor Chang Cardiac Institute of Sidney) using Lipofectamine (Invitrogene) and under the specific antibiotic selection; the positive colonies (A1 OV) were isolated and analysed.

The lines used in the technical part of this thesis are human fibroblast (FB), obtained by skin biopsy and received from Gaslini Institute (Italy, Genova). The medium culture is RPMI (Euroclone) supplemented with 18% FBS (Gibco). Cells were plated to obtain from a 50% to 90% of confluency (depending on the type of experiment to be performed) and the day after completely deprived to the serum after 2 washouts on PBS and 1 with PBS/BSA 3%. The starvation was prolonged for 5 days to avoid all the possible contribute due to cell cycle.

3.2 rt-PCR and Real-time

Total RNA from cell cultures pellets was extracted using Total RNA Mini kit (Bio-Rad) including DNase digestion. cDNA synthesis was performed using ThermoScript RT-PCR System (Invitrogen) and single-stranded cDNA analysis was done by real-time PCR using the SsoFastTM EvaGreen mix (Bio-Rad) on a CFX96 Touch real-time PCR (Bio-rad). The thermal program was set at 95°C for 5 seconds (denaturation), at 55°C for 10 seconds (annealing), 72°C for 15 seconds (elongation) for 45 cycles. The samples were normalized using the housekeeping gene Histone H3 and GAPDH.

Specific mouse primers for gene expression analysis were:

Gapdh F:cacaatttccatcccagacc R:gtgggtgcagcgaactttat

H3 F:ggtgaagaaacctcatcgttacaggcctggtac R:ctgcaaagc accaatagctgcactctgga agc

Piezo1 F:atcctgctgtatgggctgac R:aagggtagcgtgtgtgttcc

Human Piezo1 F: tgaagcgggagctctacaac R: tctcgttggcatactccaca

Map2 F: cac cag ccg ttt gag aat ac, R: gct gtt tct tcg gct gct ag

GFAP F: tcc tgg aac agc aaa aca ag, R: cag cct cag gtt ggt ttc at

FilaminA F: ggt gac gcc cgc cgc ctt ac, R: aag atg ctg g ct ggt tga cc

Vinculin F: cgt ccg ggt tgg aaa aga ga, R: aag gat tcc cct aga gcc gt

3.3 Migration assay

Cell migration assay was performed using the transwell permeable support (8 µm pores). Cells were stained with CDFA and seeded in a medium contained FBS10% and in a serum-free in the upper transwell chamber, while the lower chamber was filled with medium containing FBS 10%. After 24 hours, images of migrated cells were detected by fluoresce microscope and processed with ImageJ software.

3.4 Cell viability analysis by colorimetric MTT assay

Cell viability was evaluated by measuring mitochondrial reduction of 3-(4,5-dimethylthiazol-2-yl)-2,5-diphenyltetrazolium bromide (MTT). Cells were incubated with MTT (2 mg/ml) for 1.30h, formazan crystals dissolved in DMSO and absorbance measured at 570 nm. MTT reduction assay was also employed to measure viability of cells seeded on hydrogels 96 well glass bottom plates (Matrigen).

A1 were treated with YODA1 [0.5, 1, 5, 10µM], DMSO1% (vehicle) and with Amyloid-beta 1µM, cell viability was measured at 48h, 72h, 96h after treatment.

3.5 Immunofluorescence

Cells (differentiated, overexpressed, or wild-type) were plated on 13 mm glass coverslips and fixed with 4% ice-cold paraformaldehyde, blocked with 100 mM glycine, permeabilisated (as required) with 0.1 % Triton X-100 for 20 min. RT. After three Phosphate-buffered saline (PBS) washes, samples were incubated for 1h in blocking buffer consisting of 1% Bovine Serum Albumin (BSA) in PBS and then stained with primary antibodies; immunoreactivity was evidenced with fluorescent dyes-bound anti Ig antisera and visualized under fluorescence microscopy. Immunofluorescence dyes: Piezo1 (Abclonal), Yap (Santa Cruz), Phalloidin (Thermofisher), Hoechst (Thermofisher)

3.6 Calcium imaging

A1 cell lines were seeded in 22mm cover glass and grown for 48h in DMEM/F12 10% FBS media until 40-50% confluent. The cells were incubated with Fura-2AM for 20 minutes at 37°C in the same medium and then washed in Locke solution contained: NaCl 154mM, KCl 5.6mM, CaCl2 1.5mM, NaHCO3 3.6mM, Glucose 5.6mM, Hepes 5mM, MgCl2 1.2mM, pH 7.4. The cells were treated with Yoda1 [0.02, 0.1, 1, 2µM], DMSO (final concentration <1%) and $A\beta_{1\text{-}42}$ [1µM]. The cover glass was mounted in its holder to observe it with a microscope in a lightless room. After the chemical stimulation cells were treated with: Ionomycin to find the [iCa^{++}] saturation, EGTA to find the zero [iCa^{++}], and $MnCl_2$ to avoid all the fluorescent background due to the dye Fura2AM. The emission of fluorescence is recorded with a digital video camera connected to an image recording system. Then the images are processed with ImageJ Fiji. Data are shown as 340/380 nm ratio values and as [iCa^{++}].

3.7 Cell morphology analysis and AFM imaging

The images of A1 cells were performed by digital holography microscopy (HoloMonitor by Phiab). This technique does not require any kind of staining, since it measures of how the

cells shift the phase of light that passes through them. It is possible measure different cellular characteristic such as cell area, volume thickness, eccentricity, and cell count. Analysis was performed using HoloStudio software.

AFM analysis was carried out on $A\beta_{1-42}$ preparations aggregate at a monomer concentration of 1mM. The sample was diluted in PBS to final concentration of 50µM and was spotted on freshly cleaved mica supports at different time points (T0, T5, T24, T48).

3.8 Hydrogels preparation

Coverslips 12 mm was cleaned with milliQ water and absolute ethanol (EtOH) for 30 min each on the ultrasonic bath. Then, coverslips were silanised with an acrylsilane solution in a vacuum silanator machine, adding 300 µl of acrylsilane (alfa aesar) to a glass coverslip, placed inside the equipment, and turning on the vacuum for 3h. After silanisation, coverslips get dry at 70°C for 1h. Glass slides were made hydrophobic with a 5 min. Rainx coating. Hydrogels were prepared at three different compositions to obtain three different Elastic Moduli (0,5-1kPa, 4kPa and, 23-25kPa). These hydrogels were prepared by mixing acrylamide, bis-acrylamide and milliQ water at different proportions to achieve three different final stiffnesses. 10% (w/v) APS and TEMED at 0.1% were added to the eppendorf tube. For each 12 mm coverslip, 20µl of Hydrogels solution was poured on top of a Rainx treated glass slide and after pouring the silanised coverslip was placed on top of the solution drop to flatten it. This was left at RT for 20 min. to polymerize and then 'peeled' off the glass slide onto a 24 well plate well with 500 µl of milliQ water.

3.9 Nanoindentation

3.9.1 Experimental set-up

Nanoindentor from the Optics11 company (Nederland) called PIUMA-CHIARO is based on ferrule-top technology[53]. This instrument is composed of:

1. a controller that connects of all the components
2. an interferometer that elaborates the signal deriving from the probe
3. a head for controlling the movement where you can connect the probe
4. a PC to use the program

Figure 9 **CHIARO indenter main elements** (1) the controller, (2) the interferometer, (3) the head, (4) the pc.

The choice of the probe must take place based on the morphology or type of the cell and the level of investigation to be obtained (hydrogels, tissues, or cells). In addition, the tip must be more rigid than the sample so that its compliance can be neglected. The probe has:

- a **tip** that could be of several dimensions or geometry depending on the target
- a **cantilever,** where is allocated the tip, that bends when it approaches the cells.

- the **optical fiber** that detects the displacement of the cantilever bending analysed to the interferometer

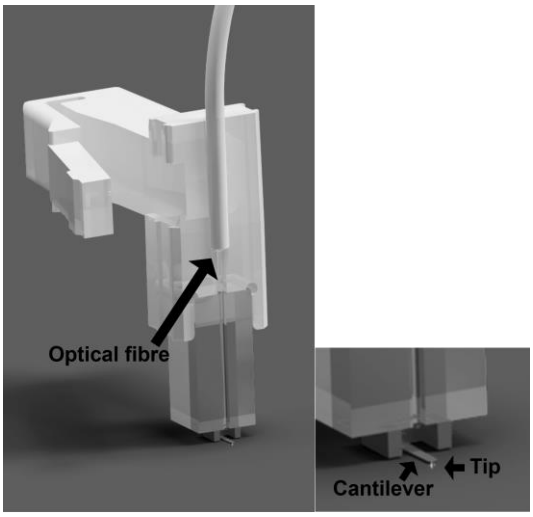

Figure 10 ***Details of a Optic11 probe***

The system is coupled with an inverted microscope and a camera, where you can monitor and control your action to a more precise measure, a characteristic not so easy in the most common indentation system, the atomic force microscopy (AFM). The relevance of a specific control is that in a non-homogeneous system like a tissue or a cell plate you can discriminate the portion and type of cell/tissue that you are approaching.

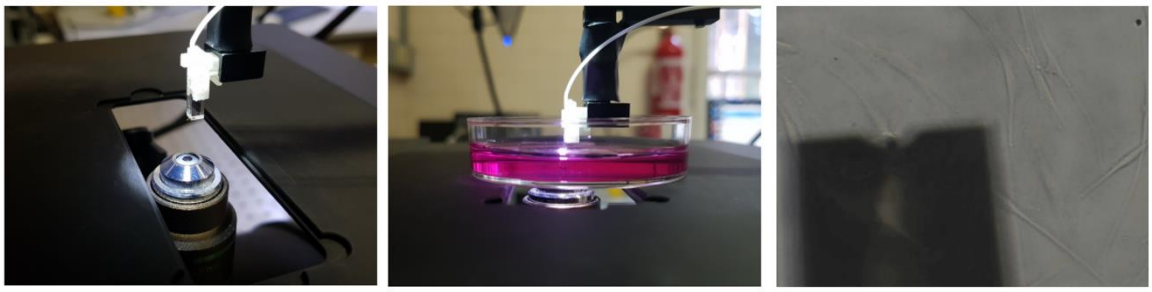

Figure 11 **View of the experimental setup** On the left, the position of the probe respect the objective. In the middle, the probe in the medium. On the right, a phase-contrast picture of the upper view of the indentation phase.

In our system, we coupled the CHIARO system with a Holographic microscope in which we added a 20x contrast phase objective.

3.9.2 Nanoindentation acquisition

We used a spherical probe with a radius of 3µm and stiffness of 0,025N/m, suitable for measuring cells in the range of 0,1-100kPa. Elasticity is expressed by Young's modulus corresponding to material stiffness, which has units of pressure.

To perform these measurements, is necessary to immerge the probe in the fluid that is used for taking measures (in our case the medium cell culture supplemented with Hepes, as pH buffer) and execute the quadrature of the probe. Then it is necessary to calibrate the probe (cantilever) to ensure correct conversion of the signal detected by the photodetector in a force value. The calibration is done by indenting a very rigid substrate (the dish's surface) and the result is the calibration factor. Now you must move the cantilever above the cell (cells are observed using a microscope associated with the nanoindenter) and approach it, moving along the z-direction, perpendicular to the sample. When the distance between the tip and the sample becomes less than 1nm (comparable to the atomic forces attractions) the cantilever is drawn towards the sample. Once in contact the tip pushes against the sample and indent it causing the cantilever bending. The indentation force applied on the cells is given by Hooke's law: $P = kc \cdot \Delta d$ (where kc is the cantilever's elastic constant and Δd its deflection). The cantilever is then retracted, but the adhesion forces make the cantilever deflects and the return force curve is different from the first one. In *Fig.12* you can see the force-displacement curves divided into three different steps. The first is the baseline where the tip is not yet in contact with the sample, the second one is the indentation curve (blue), and the third that represent the return curve (green). The zero is termed as "contact point". All the curves in which it cannot be determined are discarded.

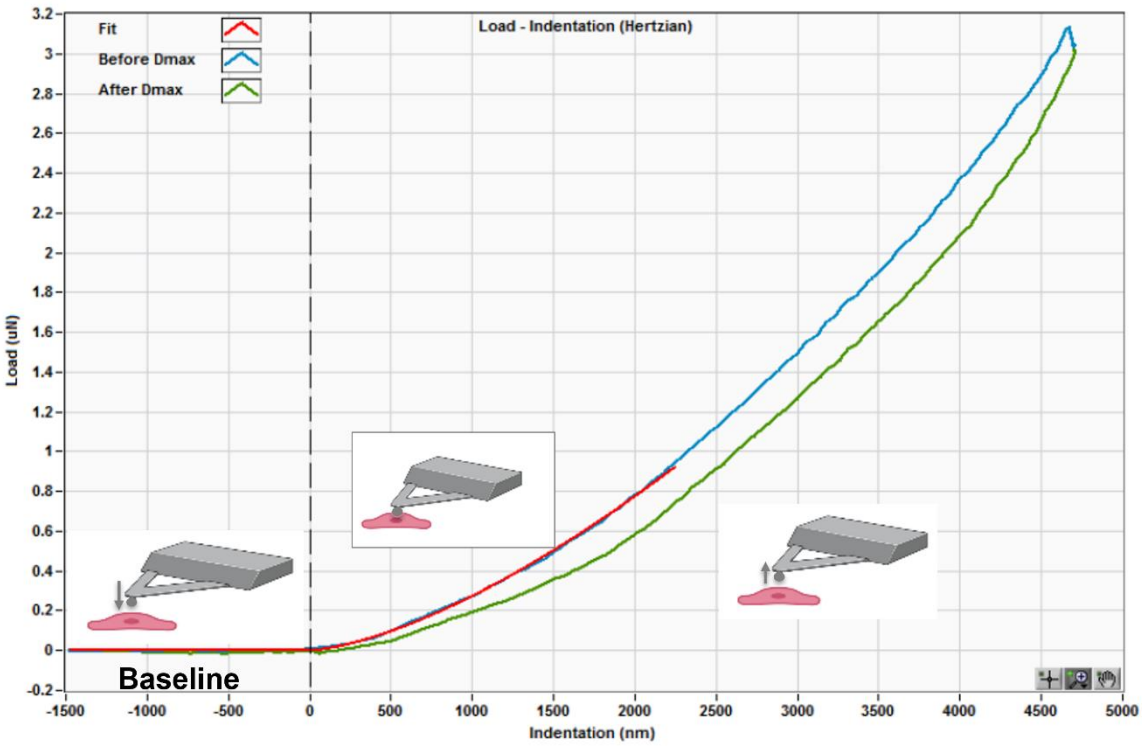

Figure 12 **Three phases of the indentation curve** The loading curve is represented in blue and is used to derive the effective Young's modulus. The unloading curve is in green and the red one is the fitting curve.

Cells were measured in standard petri dishes at 40-50% confluency with the growing medium enriched with Hepes to stabilize pH. Then, to preserve the stability of the sample, measurements were performed at room temperature and the indentations were collected for less than 1 h for each cell plate. All collected curves were analysed through a software made by Lüchtefeld *et al*. [54]. We selected only the curves to match the limit of 10% of the cell's thickness, in order to avoid the substrate, contribution to the measure.

4. CHARACTERIZATION OF THE INDENTATION CONDITIONS

Mechanical characterization of cells is acquiring much relevance, but the way and the techniques for obtaining very reliable and solid results are not at all defined. In my Ph.D. project, I used a Nanoindentor from the Optics11 company (Nederland) called PIUMA-CHIARO based on ferrule-top technology[53].

Another important consideration is that not much information about how elasticity affected cells are known. So, to standardise the indentation analysis with the PIUMA-CHIARO system, we considered a lot of possible variables that can affect the experimental results, using different lines of primary human fibroblast (FB).

4.1 STARVATION

Is already known that the phases of the cell cycle affect the elasticity of the cells, due to a continuous remodelling of the cellular shape and cytoskeleton components. So, we defined a starvation protocol (described in materials and methods) and evaluated the possible change of elasticity values in the cells we analyzed. As shown in *Fig.13* starvation causes a reduction in cell data variability, which is visible by the reduction of data dispersion. In this way, we are able to remove all higher data probably associated with the mitosis phase of the cycle. For all the following acquisitions we used only cells starved.

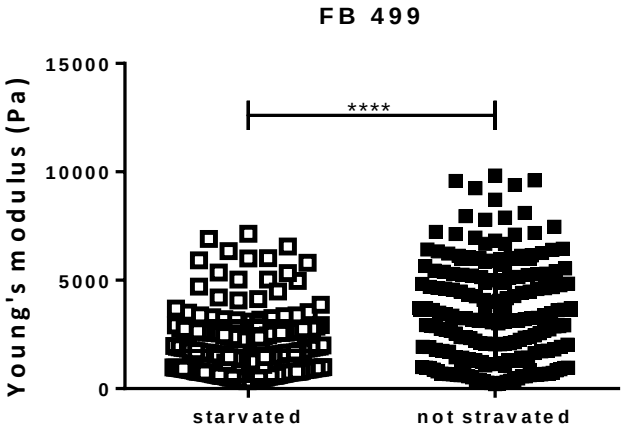

Figure 13 **Effect of starvation** The graph shows the effect of starvation in Fibroblast line 499. Dot's values represent Young's Modulus from an individual cell. The statistical analysis is on a non-parametric t-test Mann-Whitney test $p < 0.05$.

4.2 TECHNICAL REPLICATES

Usually, you should execute many measurements for conditions in such a way to have at least 100 curves, to compensate for the high intrinsic cell's variability. For this reason, you could indent the same group of cells on different days. We evaluated whether a technical replicate, that means the same cell, plated in the same moment, but analysed in two different days maintains the same elasticity values, or if one or more days in cell culture can alter the results. We tried at the beginning with two consecutive days and after with more delayed days. As you can see in the graphs in *Fig.14* the distribution of elastic values for each condition is the same and statistically, no one of these conditions incises the elasticity of three different FB lines.

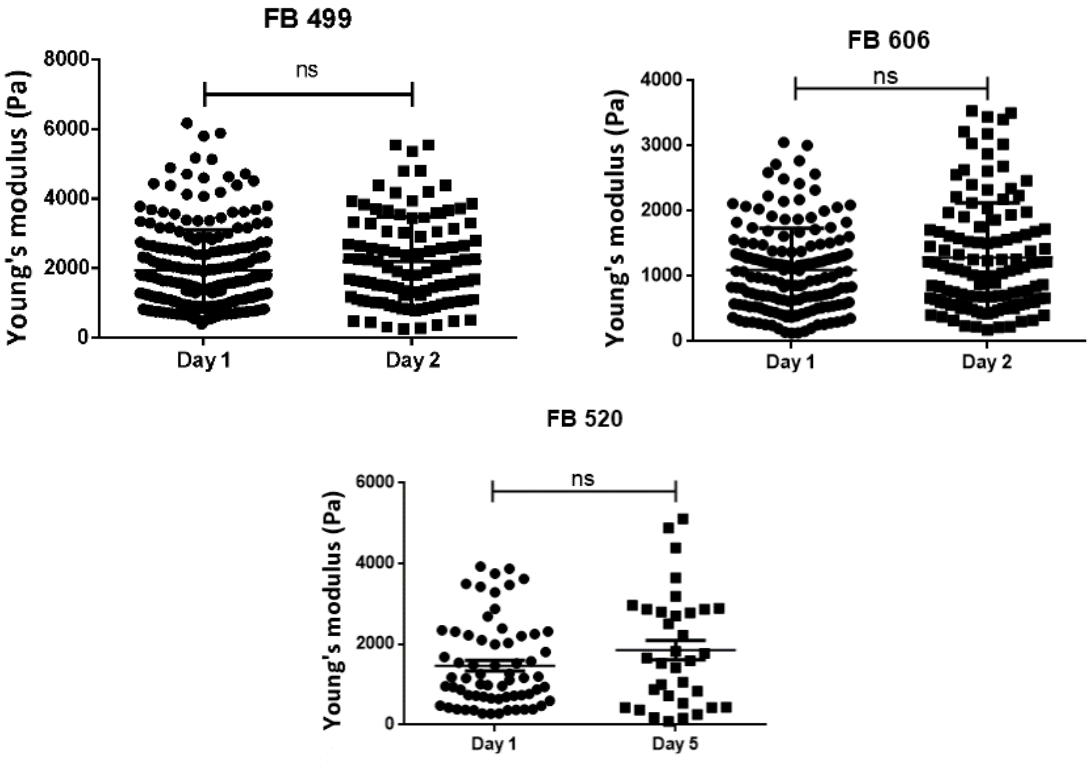

Figure 14 **Technical replication**. The graphs show the technical replication of three different Fibroblast lines 499, 606, 520. In 499 and 606 lines the technical replication was repeated after one day, in 520 after five days. Dot's values represent Young's Modulus from an individual cell. The statistical analysis is on a non-parametric t-test Mann-Whitney test.

4.3 BIOLOGICAL REPLICATES

In the same way, it could be necessary to repeat measurement in the same cell line but in different experimental moments using cells thawed from different cryovials. We compared the measurement of cells derived from different cryovials to see how stable and repeatable the analysis could be. We considered this as a biological replicate. The results in *Fig.15* show a different distribution and a statistically significant comparison in two different FB lines between their own biological replicates and in particular a reduction in elasticity that could be due to a reduction in data dispersion. Through the action of freezing and unfreezing especially in primary culture (as FB are), you select a certain type of cells at the expense of others. This under-controlled selection adding to a possible difference in terms of passages that cell lines have across different cryovials could be the reason that influences the elasticity results.

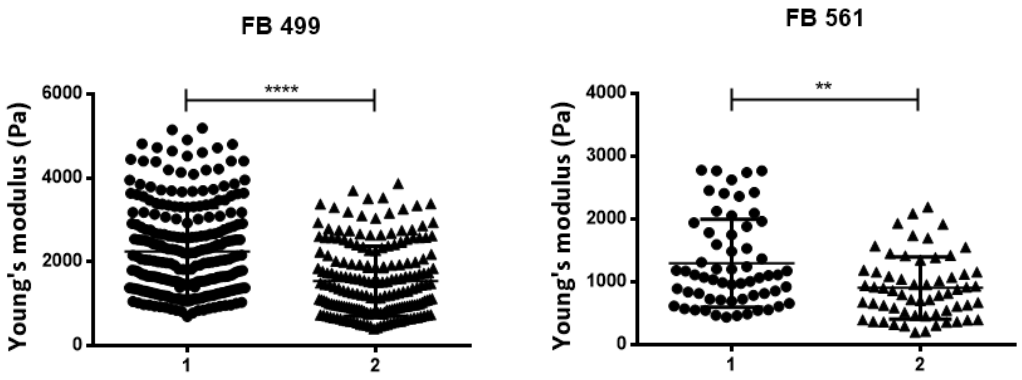

Figure 15 **Biological replication** The graphs show the distribution of the single-cell Young's Modulus, from two different Fibroblast lines, 499 and 561. The statistical analysis is on a non-parametric t-test Mann-Whitney ($p < 0.001$).

4.4 NUMBER OF PASSAGES

To underlie the possible influence of the number of passages, we executed measurement in cells across a defined number of passages. FBs we used are primary cultures so, the number of passages could be an important parameter to consider also in terms of aging. Being these lines not immortalized, passages affect the behaviours of the cells. We demonstrated that also elasticity is affected and changes across the number of passages with a particular increase under the last passage p20 (*Fig.16*).

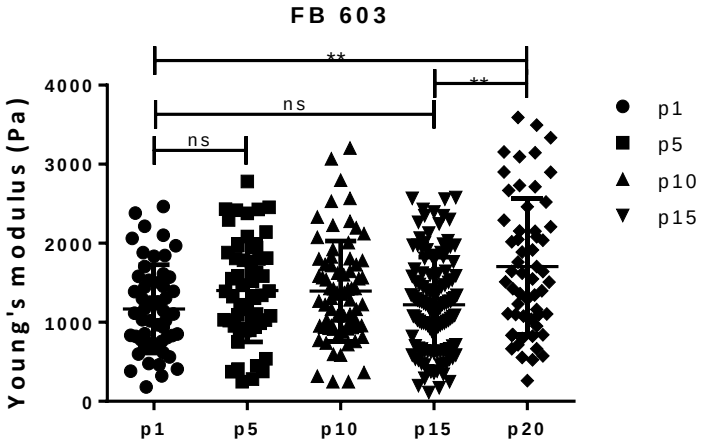

Figure 16 **Elastic modulus during cell passages** The graphs show the distribution of the single cell Young's Modulus of 603 Fibroblast line during cell passages. The statistical analysis is a non-parametric One-way ANOVA with Dunn's for multiple comparisons test ($p < 0.001$).

4.5 CELLULAR SHAPE

Cell lines are characterized by different kinds of cells despite having a single cell type in your line. In FBs we can discriminate in terms of shape two different subpopulations, cells with a flat shape from cells with a more elongated morphology (*Fig.17*). The graphs distribution showed that the different shape does not discriminate a subpopulation.

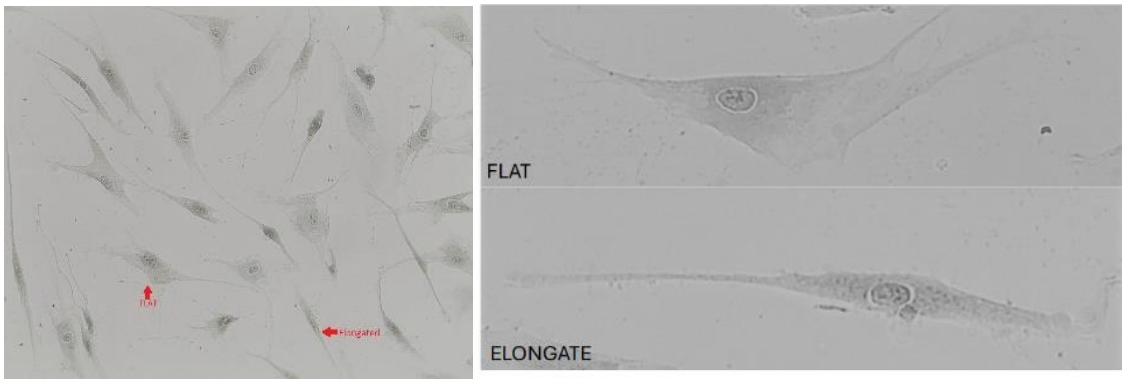

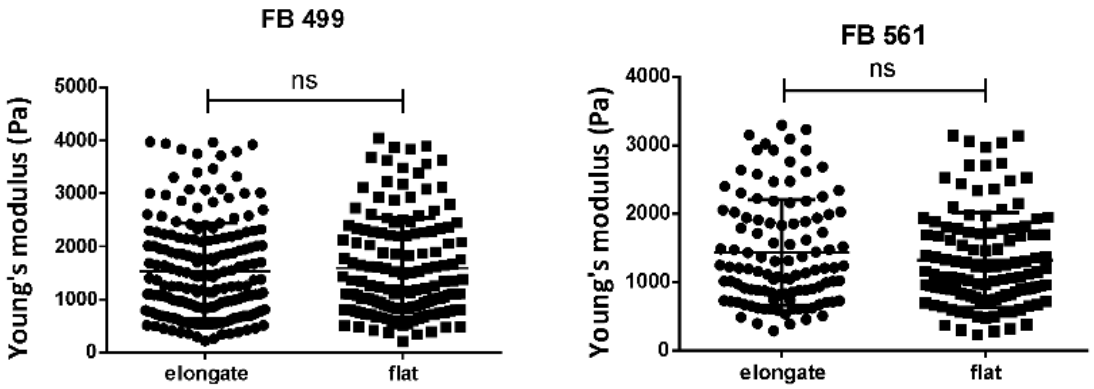

Figure 17 **Cell shape** Phase-contrast pictures evidence the presence of two different morphological population. The arrows highlight the elongate and the flat ones. The graphs show the distribution of the single cell Young's Modulus, from two different Fibroblast lines, 499 and 561. The statistical analysis is on a non-parametric t-test Mann-Whitney.

4.6 CONFLUENCY

When you design an experiment it's also important to consider the percentage of cell confluency. Several types of cells tend to form islands when plated. Cell force is different in cells in contact or isolated with other cells. And we shed light on the possible elasticity differences. As you can see in *Fig.18* we showed the confluency condition of the cells. We found that a monolayer of cells, confluency 100%, displays a strong reduction of Young's modulus in comparison to the isolated cells in two different FB lines.

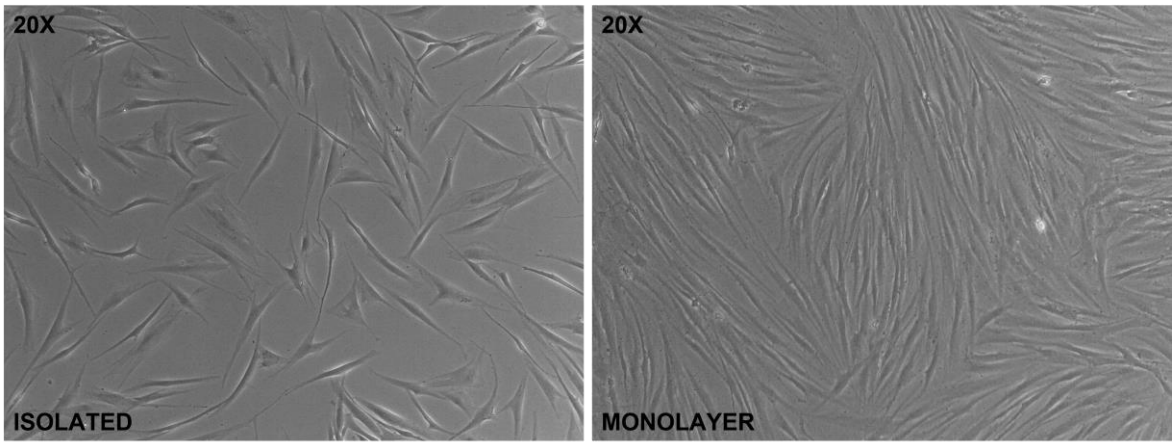

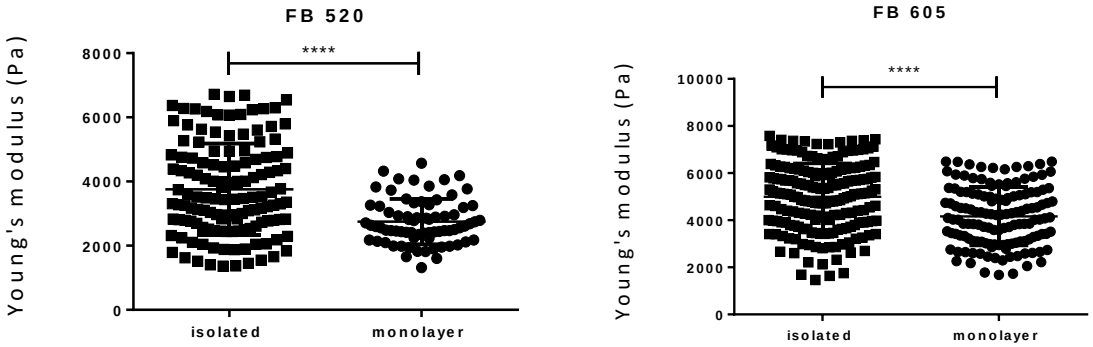

Figure 18 **Contribution of cells confluence** Phase-contrast pictures evidences the confluence state of the cell population. The graphs show the distribution of the single-cell Young's Modulus, from two different Fibroblast lines, 520 and 605. The statistical analysis is on a non-parametric t-test Mann-Whitney.

Then we analysed through the 3D imaging microscope, coupled with our CHIARO system, the thickness parameter of this cell condition. We found out that, when cells are plated with a very high rate of confluency, displayed an increase in thickness value that could be related to the reduction of Young's modulus.

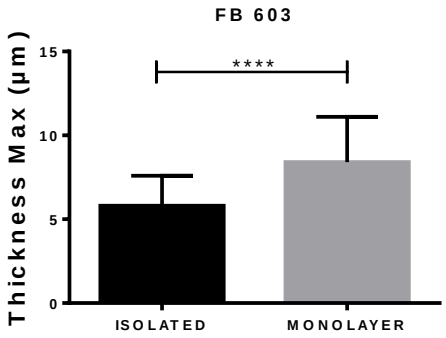

Figure 19 **Morphological evaluation** The thickness of FB line 603 was calculated by holographic microscopy. The histogram represents the medium value of the thickness of 100 cells and 40 islands/monolayers of cells. The statistical analysis is on a non-parametric t-test Mann-Whitney ($p<0.001$).

From this in-depth characterization we conclude that results in nanoindentation experiments depend on many confounding factors and experimental conditions. In order

to obtain comparable results, it is necessary to have a great accuracy carrying out the experiments, choosing the experimental conditions and designing the algorithms. However, because nanoindentation experiments does not follow a standard protocol, every absolute result is hardly comparable within different research groups. Anyway, if experiments are carefully planned and experimental conditions are kept constant, then relative results are comparable.

5. RESULTS

5.1 DIFFERENTIATION OF A1 CELL LINE

A1 cell line is a good neuron *in vitro* model because displays both indefinite proliferation and neuronal features that can be increased upon differentiation. We have employed the neural differentiation protocol of A1 cells previously described by *Colucci et al.* (see Materials and Methods) [52]. Indeed, after 5 days of differentiation, the cells showed an increase in axons length visible in *Fig.20* (A, B).

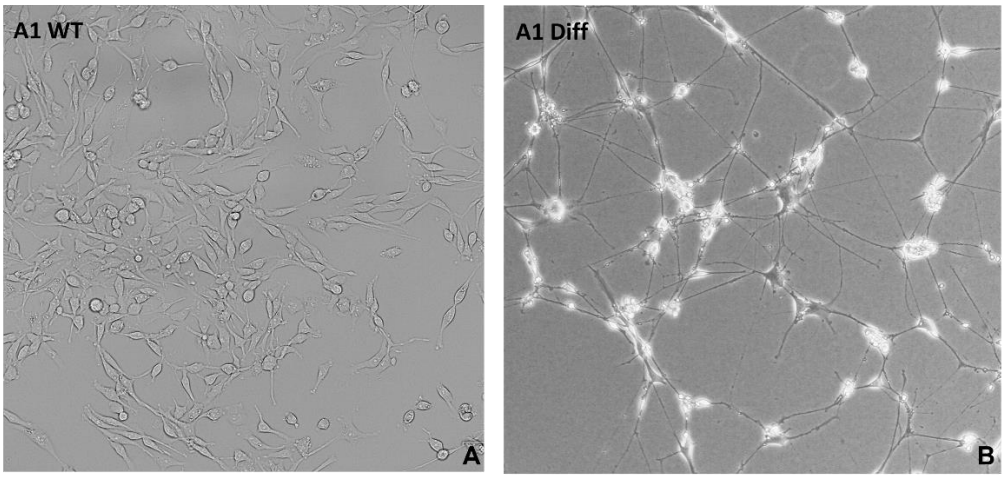

Figure 20 **Phase-contrast photomicrographs** A1 cells after 5 days in the presence of 10% FBS appear flat and large (A, 10x). A1 cells grown for 5 days in serum-free medium supplemented with 1 mM cAMP show a morphological change, all cells show multiple neurites sprouting from cell body (B, 10x).

We evaluated by real-time PCR, the gene expression levels of the mechanosensitive ion channel Piezo1 in this cell line. The data show that Piezo1 is expressed in A1 cells, but its expression rate is not so high as compared to housekeeping genes *GAPDH, H3*. More in detail, we also demonstrated that Piezo1 expression decreases upon differentiation. We also tried to execute a Western blot (WB), a quantitative measurement of the protein content in cells. Due to the large size of Piezo1 protein, as previously described in detail, adding to the low gene expression, it was not easily performing a reliable WB. Thus, we could only perform immunofluorescence labelling, which has confirmed the presence of Piezo1 in WT and differentiated A1 cells (*Fig.21*).

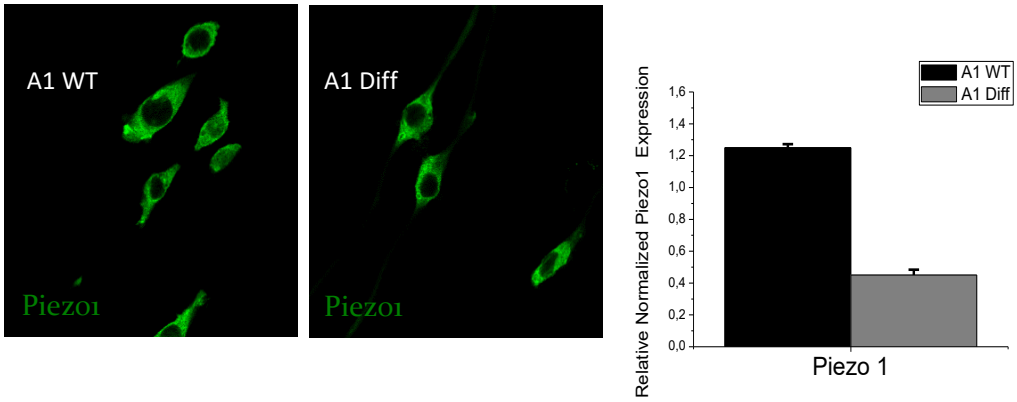

Figure 21 **Piezo1 expression and immunofluorescences of WT and differentiated A1 cells** By Real-Time PCR we confirmed the presence of Piezo1 gene, and that Piezo1 expression levels decrease upon differentiation of A1 WT cells. GAPDH and H3 were used as internal standards (left). The expression of Piezo1 was confirmed by immunofluorescence with antibody against Piezo1 in WT and differentiated A1 cells (right).

In order to address the activity of Piezo1 channel, we tested the effects of chemical activator Yoda1 at different concentrations on A1 cells. First of all, by means of MTT assay, we checked several dilutions to choose the range of Yoda1 concentrations that do not affect cells viability, to be used in the following experiments. Yoda1 is only soluble in DMSO so, we used a standard internal control medium containing less than 1% [DMSO] corresponding to the amount added with 0.5, 1, 5, 10µM Yoda1 in the medium. The data showed that Yoda1 inhibited cell proliferation in a dose-dependent manner and the concentrations that do not statistically affect viability range from 0.5µM to 1µM (*Fig.22*).

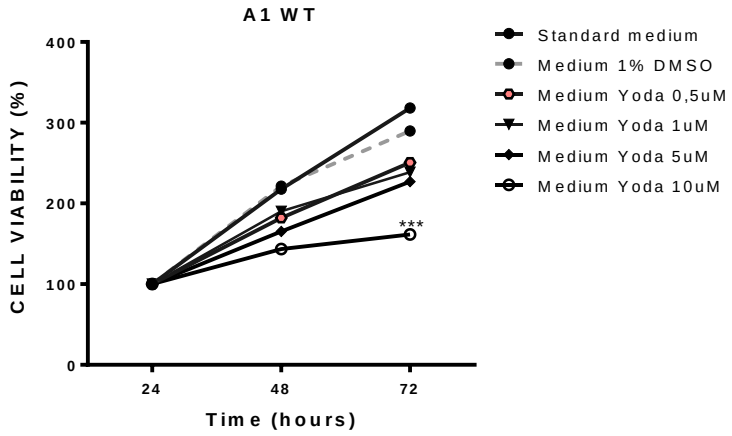

Figure 22 **MTT assay with Yoda1 stimulation** Cells proliferation was evaluated by MTT reduction test. Values, taken as a percentage of the value at time 24hrs, are the average of two independent experiments, performed in quadruplicate (*p<0.01 Yoda 5µM vs. standard medium and ***p<0.01 Yoda 10µM vs standard medium).

Then we performed a single cell calcium-imaging assay to evaluate the functional activity of Piezo1 channel. The addition of Yoda1 evokes a rapid increase in intracellular calcium ions (i[Ca^{++}]), underlying, the presence of functionally active Piezo1 channels in the plasma membrane of the cells. We used different concentrations of Yoda1 to create a dose-response curve in WT and differentiated A1. The curves show that differentiation affects A1 response to Yoda1. Indeed, while in undifferentiated cells i[Ca^{++}] rises linearly as [Yoda-1] increases, in differentiated A1, i[Ca^{++}] increase is lower and not linear (*Fig.24*). This evidence indicated that A1-WT cells are a more stable and adjustable model for pharmacological treatment and for investigating the function and signalling of Piezo1 channel.

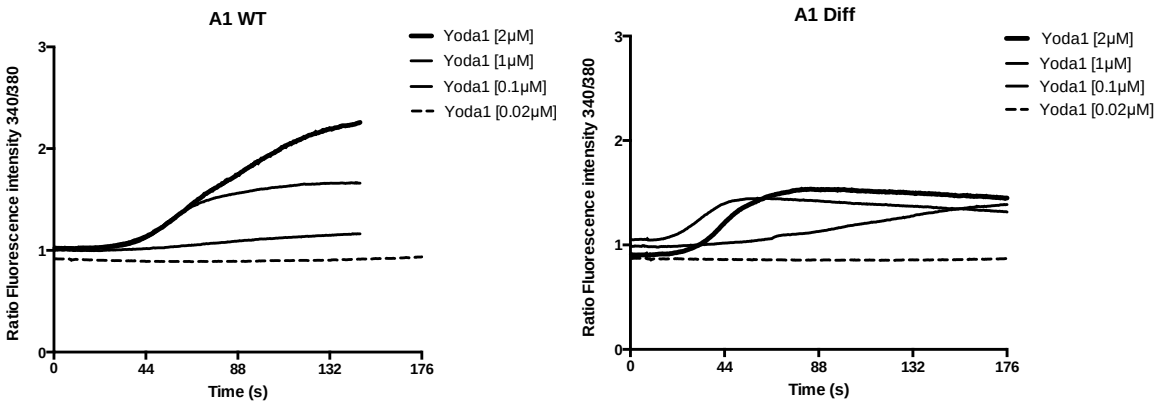

Figure 23 **Calcium imaging assay** Fura-2 ratiometric images showed changes in the cytosolic Ca^{2+} concentrations after acute YODA1 injection in WT (left panel) and differentiated A1 (right panel).

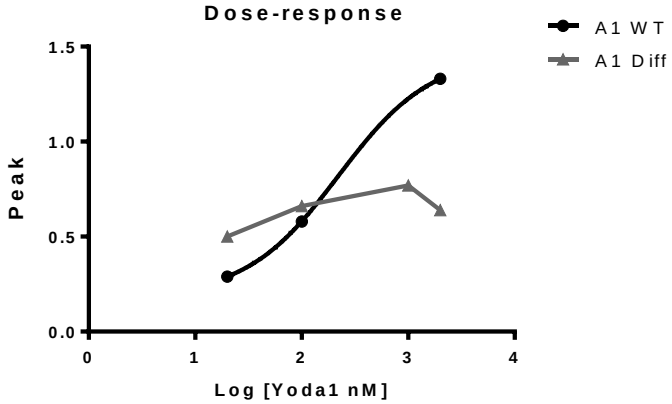

Figure 24 **Dose-response curve.** The graph shows the medium of single cells' response to stimulation by the agonist Yoda1. In A1 WT cells as Yoda1 increases, the response rises in a relatively linear manner compared to differentiated A1 cells.

5.2 OVEREXPRESSION OF PIEZO1 IN A1 CELL LINE

Quantitatively, gene expression of Piezo1 in A1 cells is relatively low if compared to the standard internal control GAPDH or H3 (as housekeeping genes). To have a better read-out in the following experiments, we were able to create a new cell line in which Piezo1 is overexpressed. An expression plasmid containing human Piezo1 ORF was obtained by Cardiac Research Institute of Sydney and stably transfected in A1 cells. Through Real Time PCR experiments, we confirmed the high expression of the human-Piezo1 gene in A1 (A1 OV) cells (*Fig.25*).

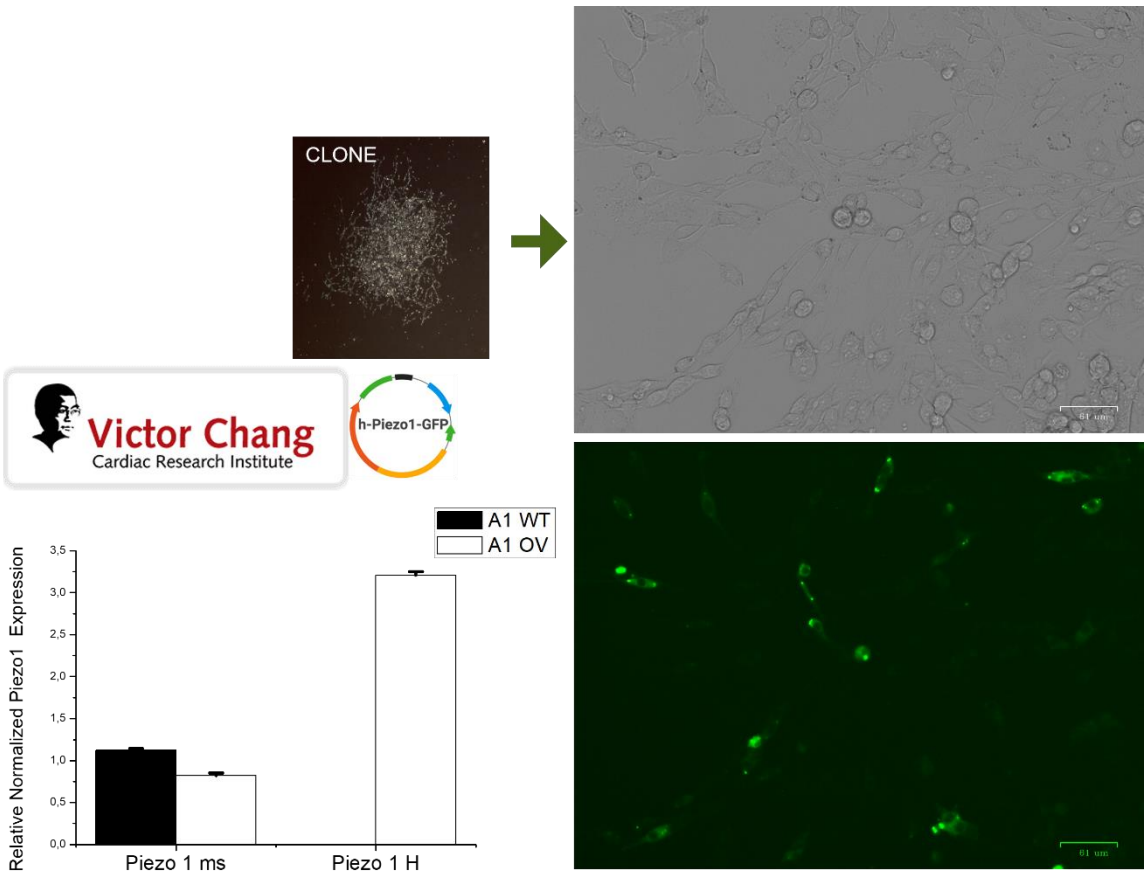

Figure 25 **Piezo1-overexpression in A1 cells** Using the human-Piezo1-GFP plasmid received from Cardiac Research Institute of Sydney was created a new cell line in which Piezo1 is overexpressed; the human-Piezo1 gene presence was confirmed by Real-Time PCR. Diagram express the relative level of h-Piezo1-GFP mRNA analyzed, compared to the internal standard GAPDH and H3. On the right, GFP fluorescence detection of transfected clones.

WT e OV A1 cells were morphologically compared through 3D imaging using a holographic microscope. This analysis shows that WT and Piezo1-overexpressing A1 diverge in terms of area and thickness. The analysis is based on the observation of 500 cells of each different type. A1 OV cells have a thickness average between 3,1 and 7,3µm and an area ranging between 100 and 500 μm^2. In contrast, A1 WT cells have a thickness average of 1,7-4,5µm and an area of 260-740 μm^2. Thus, we can conclude that A1 OV cells, compared to A1 WT, are thicker in a smaller surface area.

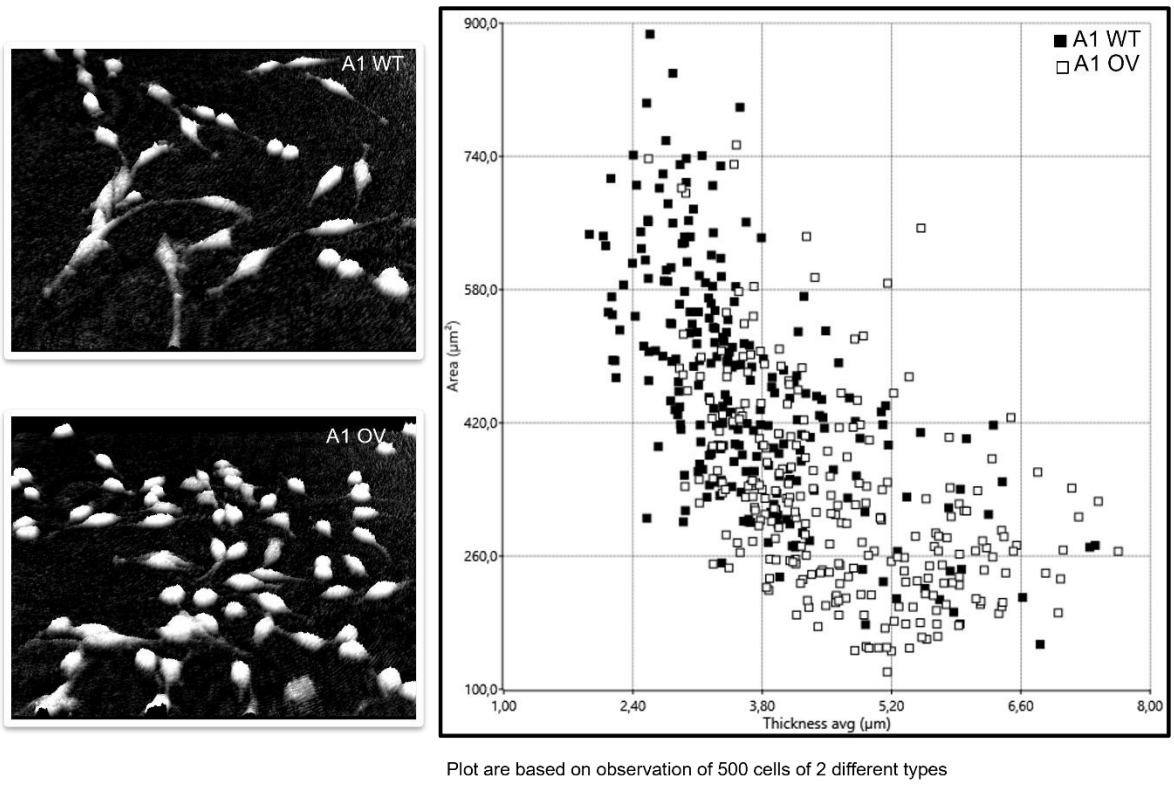

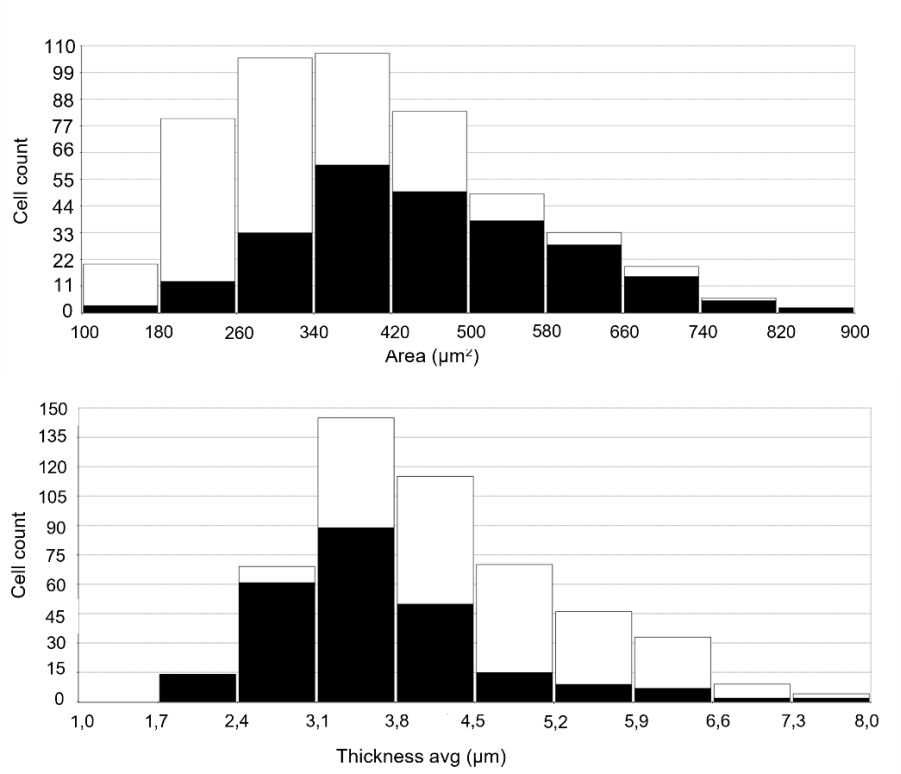

Figure 26 **Piezo1 overexpressing cells posse a different cellular shape**. Cells were compared morphologically through 3D images obtained with a holographic microscope (Phiab). A1 cells diverge in terms of area and thickness. The analysis is based on the observation of 500 cells of two different types. The scatter plot and the histograms show that A1 OV cells are thicker in a smaller surface area compared to A1 WT.

It is known that Piezo1 is involved in the regulation of cell motility, thus we compare WT to OV A1 cells in a migration assay to. The results showed a slight, albeit not significant (-25%), reduction of cell migration in A1 OV as compared to WT cells (*Fig.27, left*).

We then observed a difference in the growth curve between non-transfected and Piezo1-transfected A1 cells. The analysis of cell proliferation, obtained by MTT assay after 72 and 96 hours, shows that the growth rate of A1 OV is significantly reduced when compared to A1 WT (*Fig.27, right*); however, no signs of cytotoxicity in A1 OV were detectable at any time point analyzed. These data underlie that the over-expression of Piezo1 modifies the proliferation rate of A1 cells.

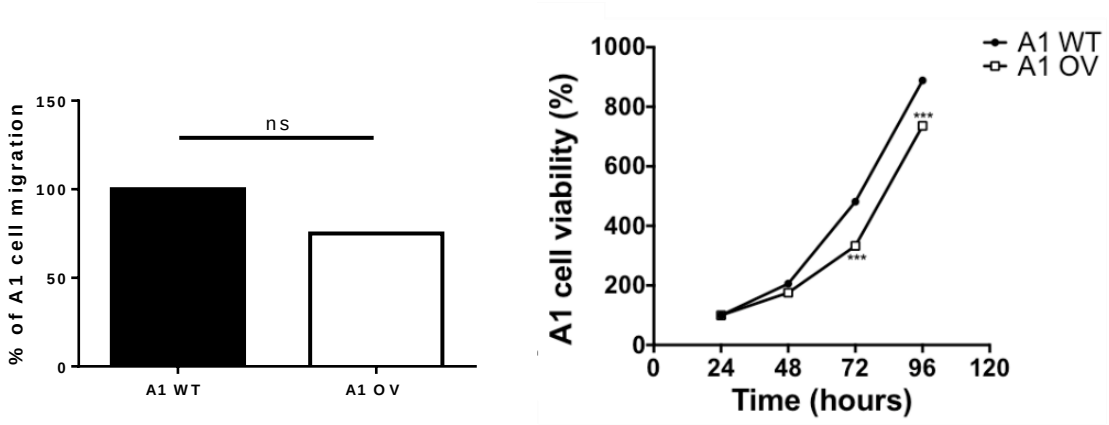

Figure 27 **Piezo1 overexpressing cells have a reduction in migration and viability** Transwell migration assay of WT and OV A1 was performed by staining with CDFA and seeding in serum-free medium in the upper transwell chamber, while the lower chamber was filled with medium containing FBS10%. After 24 hours, images of migrated cells were detected by a fluorescence microscope. The results showed a slight not significant (25%) reduction in A1 OV compared to WT cells (left). Viability assay performed by MTT reduction test of WT and OV A1 cell lines (right). Values taken, as a percentage on time 24hrs are the average of two independent experiments, performed in quadruplicate (***$p < 0.01$ A1 OV vs. A1 WT).

As previously discussed, Piezo1 activity was proposed to be modulated by changing cytoskeleton composition, and its differential expression could influence cell fate. Thus we performed a Real-Time PCR analysis to evaluate possible changes in the expression of some cytoskeleton and differentiation-related elements. Using as internal control the expression of these genes in A1 WT it is evident that the overexpression of Piezo1 leads to an

overexpression of genes linked to differentiation like GFAP and Map2 and structural genes such as Vinculin. On the contrary, FilaminA does not have a significant upregulation (*Fig.28*).

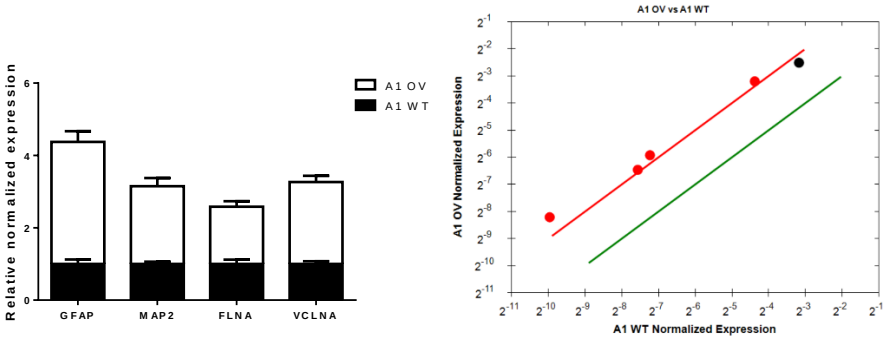

Figure 28 **A1 OV upregulates the expression of some cytoskeleton elements** The histogram shows the differential expression of A1 OV cell line using the expression of A1 WT cells as a standard internal control. GAPDH and H3 were used as internal standards. On the right are the statistical differences in terms of fold-changes (red dots for up-regulation).

As subsequent step, we compared the mechanical properties of wild type (WT) and Piezo1 overexpressing (OV) A1 mesencephalic cells, using the nanoindenter Chiaro-Piuma. We performed single-cell nanoindentation experiments to obtain information about single-cell elasticity. For each cell line more than 200 indentation curves were acquired. We used two different models for the analysis of the curves: the first one, based on Hertzian model, provides the Young's modulus of each single cell considering it as a homogenous system. On other hand, the second model allows an elastography analysis, which considers the cells as a non-homogenous system, granting the possibility to distinguish two different layers of elasticity: a bulk (referred to cytoplasm) and a cortex (referred to actin cortex).

In *Fig.29 (a)* the calculation of the Young's module is reported, showing that the overexpression of Piezo1 induces a modest stiffening of the cells, which did not reach statistical significance between the two cell lines.

As far as elastography analysis, *Fig.29 (b-c)* shows that overexpression of Piezo1, when compared to A1 WT cells, induces stiffening mainly on the cortex, while causes a softening of the bulk.

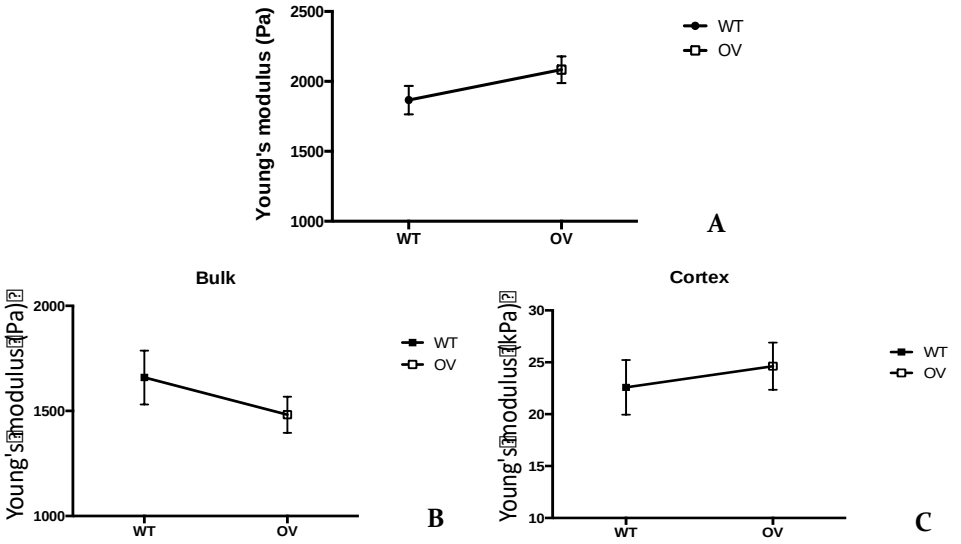

Figure 29 **Elasticity of A1 cell line** The graph shows the differences of the Young's modulus mean value of 100 curves taken with the Nanoindentor. Hertzian model considers cells as a homogenous system, showing one Young's modulus value for each cell line (A). Elastography software analysis considers cells as a non-homogenous system, and you can see the Young's modulus of the bulk (B) and of the cortex (C) for each cell line.

Then we performed a single cell calcium-imaging assay to evaluate the functional activity of the Piezo1 using different concentrations of its agonist Yoda1, to create a dose-response curve in WT and OV A1 cells. The curves show that channel overexpression enhances A1 response to Yoda1 which is detectable at lower concentrations, although when the [Yoda-1] increase the response tend to even out. This evidence indicated that A1 OV cells are more sensible at lower [Yoda-1]. On the other hand, higher Yoda-1 potency was observed in A1 WT with an EC_{50} of 121 nM as compared to 786 nM in A1 OV.

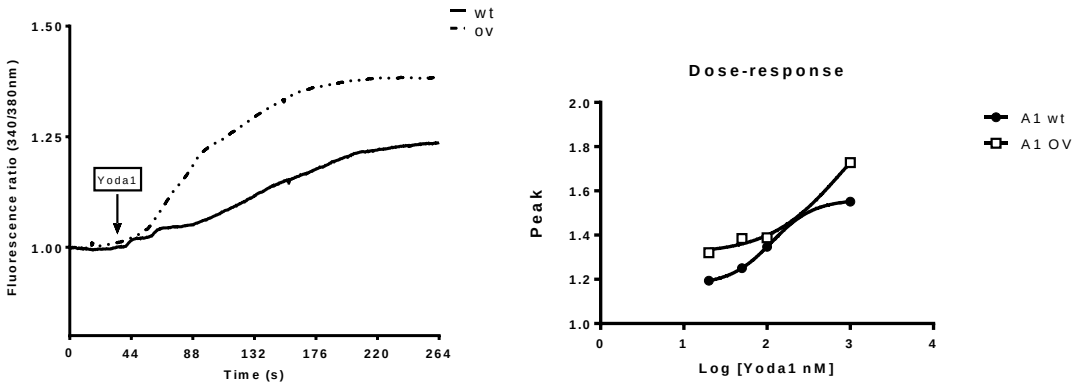

Figure 30 **Calcium imaging assay and dose-response curve.** Fura-2 ratiometric images showed changes in the cytosolic Ca^{2+} concentrations after acute YODA1 injection in WT (black line) and A1 OV (dashed line) (left). The graph shows the medium of single cells' response to stimulation by the agonist different [Yoda1].

5.3 SUBSTRATE'S CONTRIBUTE

Substrate stiffness can influence several biological features of cells, and even the lineage destiny, as previously described. Thus, to better characterize the mechanical properties of the cells we are studying and the role that Piezo1 could play, we used specific multiwall and dishes from Matrigen®, composed of hydrogel with different stiffness coated with Collagene1.

First of all, we used a multiwell plate composed of columns of wells coated with Matrigen covering stiffness from 0.2, 0.5, 1, 2, 4, 8, 12, 25, to 50 kPa, with 3 columns, used as internal controls, that have a stiffness of standard cell culture plasticware. In this analysis we were interested to verify whether A1 WT or A1 OV adopts a different behavior in a range of substrates from very soft to highly stiff.

Our first observation indicated that soft substrate affected lateral sprouting of cytoplasm in both A1 cell types indicating a possible impairment of neurite growth, independently from the levels of Piezo1 expression.

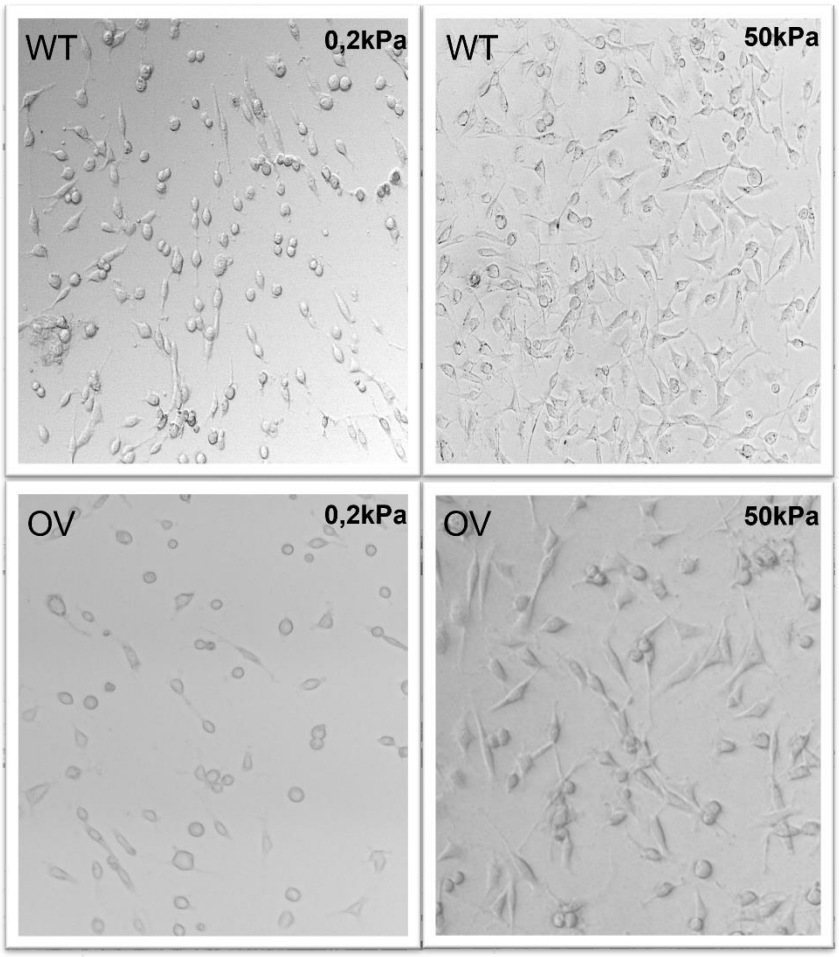

Figure 31 **Phase-contrast images** A1 cell line plated in a substrate soft as 0.2kPa defect in lateral sprouting of cytoplasm.

Then, we evaluated cell proliferation rate in the different Matrigen substrates, using the MTT assay. The data obtained indicate that both cell lines grow slower in softer than in stiffer substrates such as plastic, the growth increases in parallel with substrate stiffness regardless of the amount of Piezo1 expressed.

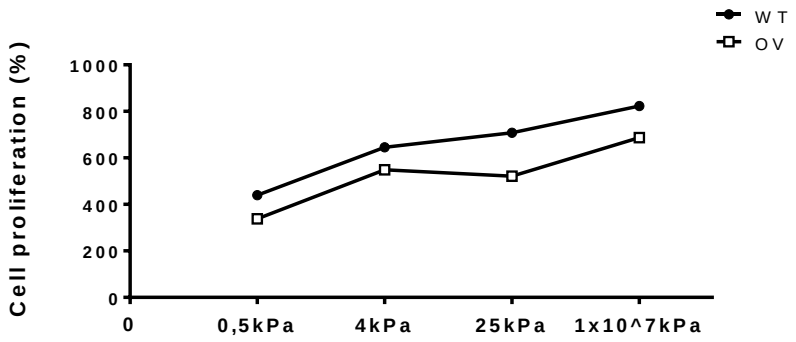

Figure 32 **Cell viability** Viability assay performed by MTT reduction test of WT and OV A1 cell lines. Viability values have been measured after three days of proliferation and expressed as a percentage on time 0 to 72hrs.

To quantify the shape differences induced by the substrate in which cells are growing, we used a holographic microscope and compared cell morphology. This instrument allowed us to characterize cells in term of area, thickness, and eccentricity. We got around 100 pictures for each cell condition; cells were plated on substrates with 0,5kPa, 4kPa, 25kPa and on glass. This analysis shows an effective changing in cell shape depending on the substrate on which cells are plated. A1 WT 0,5kPa have an area mean of 221-410µm^2, A1 WT 4kPa 348-507 µm^2, A1 WT 25kPa of 281-450µm^2 and A1 WT cells of 358-549µm^2. The thickness maximum is respectively: 7.5-9.6µm, 6.7-8.7µm, 6-8.5µm, and 6-9µm. These data underlie that the stiffness of the substrate influences cell shape and, considering only soft substrate, the thickness increases when the substrate becomes softer (*Fig.33*).

Another relevant parameter we analysed is eccentricity. It underlies how elongated the cells are, or how much the cells deviate from being a sphere. More elongated cells are, eccentricity value becomes higher, approaching 1; more cell shape resembles a sphere, the values approach 0. Cells plated in a softer substrate and cells in which Piezo1 is overexpresses are more eccentric than A1 WT cells plated in a stiffer substrate (*Fig.33*).

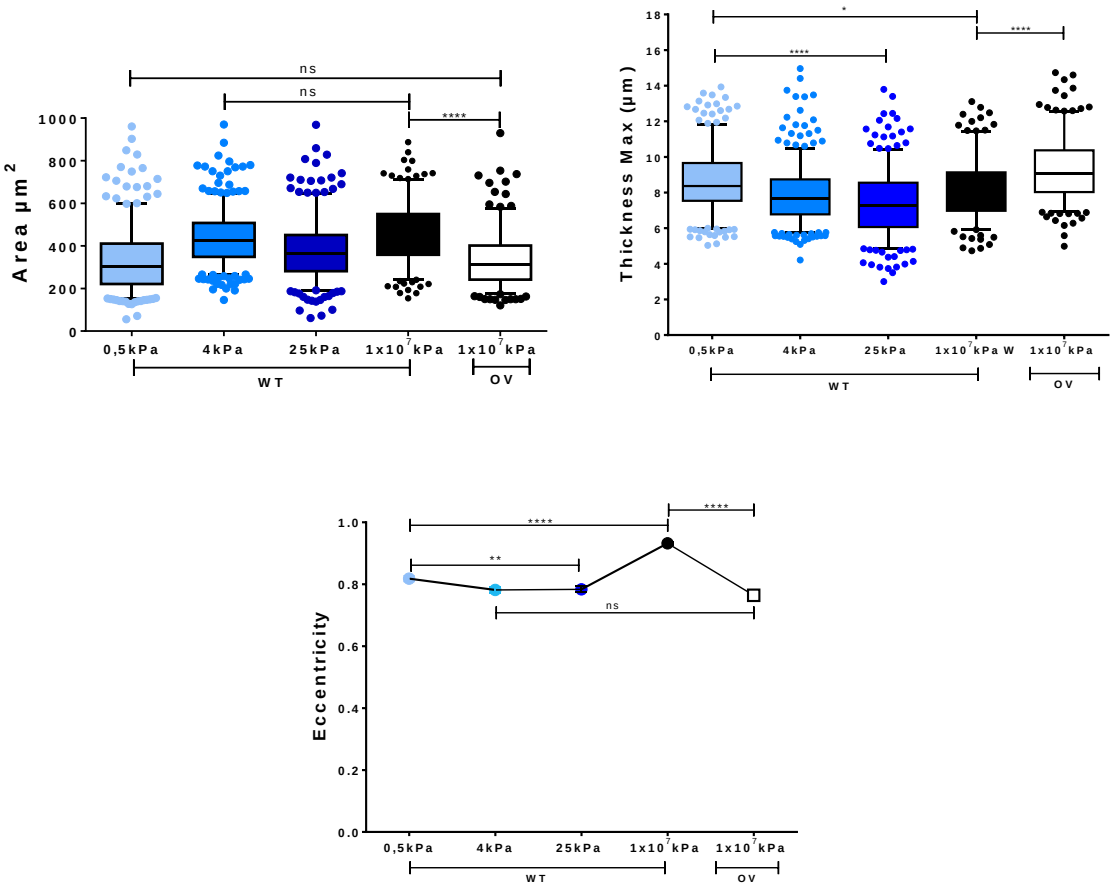

Figure 33 **Analysis from 3D images obtained with a holographic microscope**. This analysis is based on observation of 200 cells, plated on the four different substrates. (****<0.001 *p-value* One way ANOVA and Tukey's multiple comparison test)

To verify whether these differences reflect Piezo1 function changes, we performed a single cell calcium-imaging assay, evaluating whether the sensibility of the channel to its agonist Yoda-1 changes according to substrate stiffness. To do this, we performed an acute administration of Yoda1 on A1 WT cells plated to a glass (over $1x10^7$kPa), 0,5kPa, 4kPa, and 25kPa substrate. The *Fig.34* shows that a softer substrate sensitized Piezo1 activity in A1 WT cells.

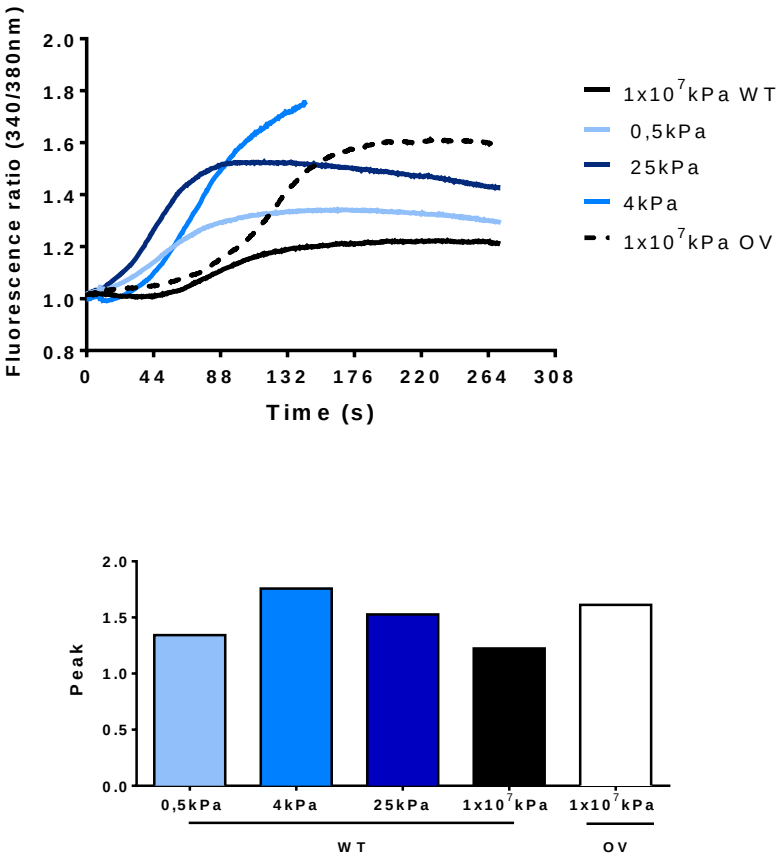

Figure 34 **Single-cell calcium imaging with Yoda1 stimulation** Yoda1 [0.05µM] elicits bigger calcium rises in A1 OV cell line and in A1 WT in a softer substrate. The curves represent the average single-cell response expressed by fluorescent ratio intensity 340/380. In the graph below is the representation of the medium value of the peak that cell acquired in each experimental condition

To understand whether this higher response could be related to a different intracellular calcium concentration we created an algorithm to convert the fluorescent ratio 340/380 curves obtained by microfluorimetric analysis in [iCa^{++}] using the Grynkieicz equation. To accomplish this task, at the end of each calcium imaging experiment, the curve generated by fluorescent ratio 340/380 have to be calibrate using three different compounds: Ionomycin to identify the [iCa^{++}] saturation Fura2, EGTA to find the zero [iCa^{++}], and $MnCl_2$ to avoid all the fluorescent background due to the dye Fura2AM.

$$[Ca^{2+}] = k_D^B \left(\frac{R - R_{min}}{R_{max} - R} \right) \left(\frac{S_{f2}}{S_{b2}} \right)$$

Figure 35 **Grynkieicz equation**

Then we analyzed through ImageJ software the fluorescence ratio 340/380, and, using the program we developed as an excel sheet, we converted the curves in [iCa^{++}]. As you can see in Fig. A1 OV cells have a higher basal [iCa^{++}] compared to A1 WT cells plated on glass, but similar concentrations were observed when A1 WT cells are plated in a soft substrate (e.g. 4kPa and 25kPa). As far as 0,5kPa condition, we could not obtain enough cells to be analysed to have statistically relevant information.

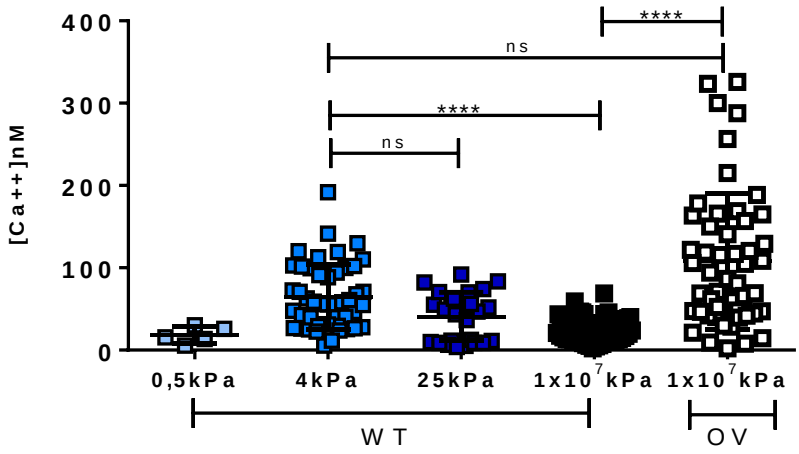

Figure 36 **Single-cell basal [iCa^{++}]** The intracellular basal calcium concentration was calculated using Grynkieicz equation to transform the data of the single cell calcium imaging assay, expressed as fluorescent ratio 340/380. Dots represent the values of individual cells (****<0.01 *p-value* One-way ANOVA and Tukey's multiple comparison test)

A useful tool to measure mechanotransduction is the quantification of the activation of the transcriptional factor YAP, indirectly evaluated by its nuclear translocation. To evaluate whether mechano-transduction is affected in response to changes in substrate stiffness and over-expression of Piezo1, YAP nuclear translocation was measured. Representative images of this experiment can be seen in *Fig.37*, where YAP is mostly excluded from the nucleus of cells plated in a softer substrate but not in A1 WT or A1 OV cells plated on glass.

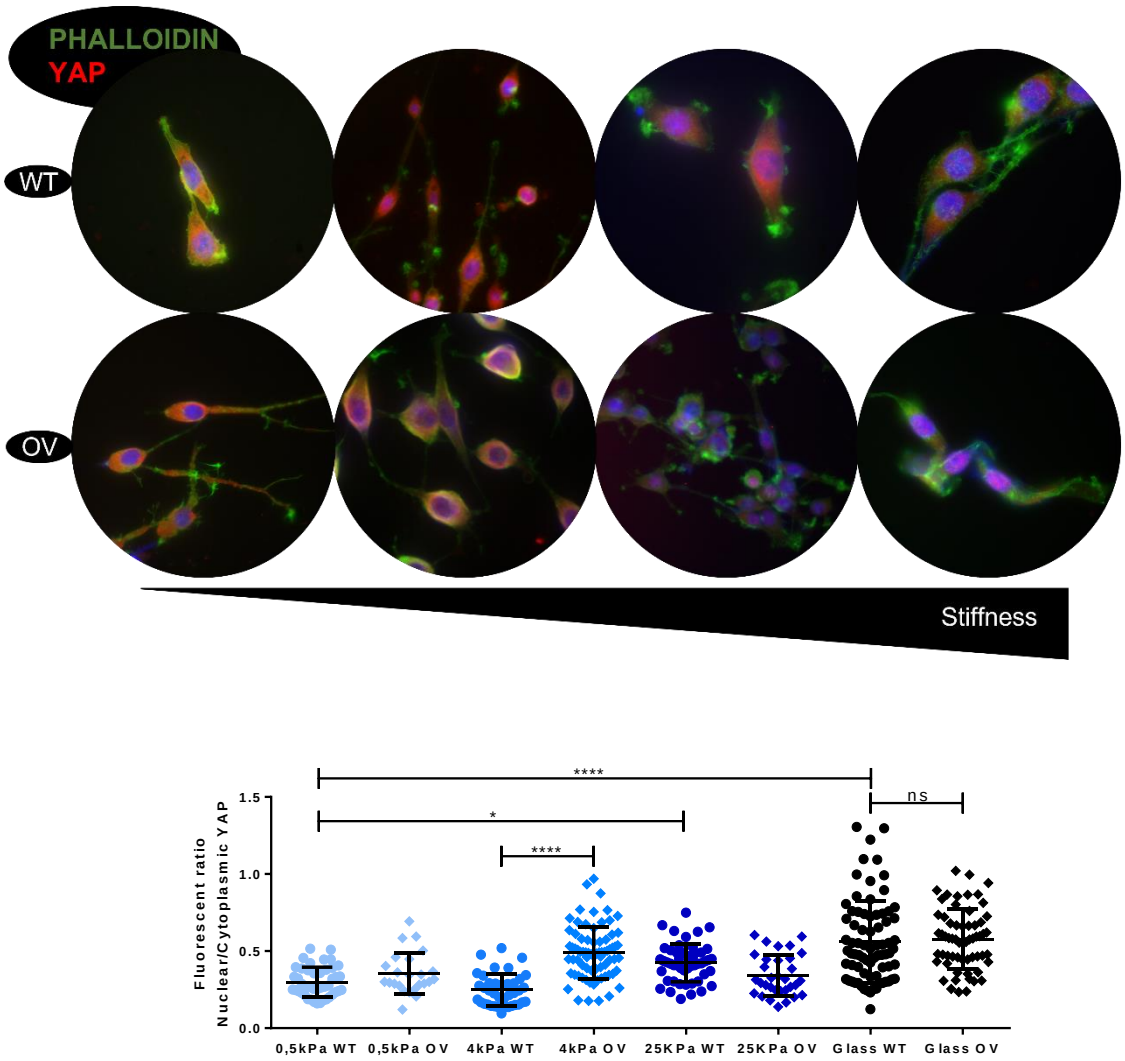

Figure 37 **Representative imaging and quantification of Yap** Representative cell images where YAP, cell profiler, and nucleus can be observed by an immunolabelling YAP (red), Phalloidin (green), and DAPI (blue) stain. In the graph below you can see the nuclear/cytoplasmic YAP ratios quantified by ImageJ analysis. The graph is organized by cell type and substrate condition. Dots represent values for individual cells (****<0.01 *p-value* One-way ANOVA and Tukey's multiple comparison test)

We also compared the mechanical properties of A1 WT and A1 WT cells plated in a softer substrate using the CHIARO nanoindenter. As reported in Fig.38, the stiffness of the cells is influenced by the stiffness of the substrate: it increases with the increase of the substrate stiffness.

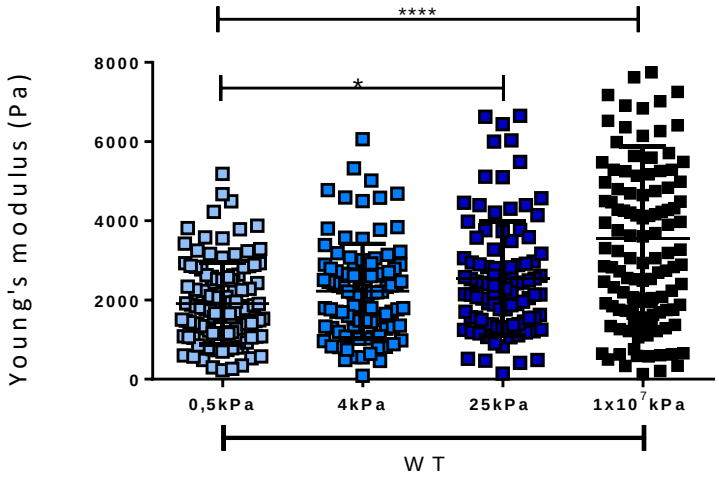

Figure 38 **Elasticity of A1 cell line** Cells stiffness is influenced by the stiffness of the substrate. The elasticity of A1 cell line is measured by the nanoindenter CHIARO (Optics11). The graph shows the differences of Young's modulus mean value of 100 curves for each stiffness condition. Dots represent values for individual cells (****<0.01 *p-value* One-way ANOVA).

Following these results, we performed a Real-Time PCR analysis to verify whether stiffness variation could also modify the expression of cytoskeleton elements and differentiation-related markers, such as FilaminA, Vinculin, Map2, and GFAP. To this purpose, we analysed the expression of such parameters after ten days from the plating of WT and OV A1 cells on standard plasticware or substrates with different stiffness. The graphics in *Fig.39* show that the stiffness of the substrates does not influence the expression of most of these genes in WT cells, with the only exception of GFAP which was upregulated when cells are grown on a soft substrate (4kPa). In contrast, the overexpression of Piezo1 influenced in more marked way the expression of GFAP on cells plated in 4kPa substrate and FlmnA and VNLA on cells plated in 25kPa substrate which, however, were downregulated. Interestingly, in these conditions the expression of Piezo1 itself was reduced.

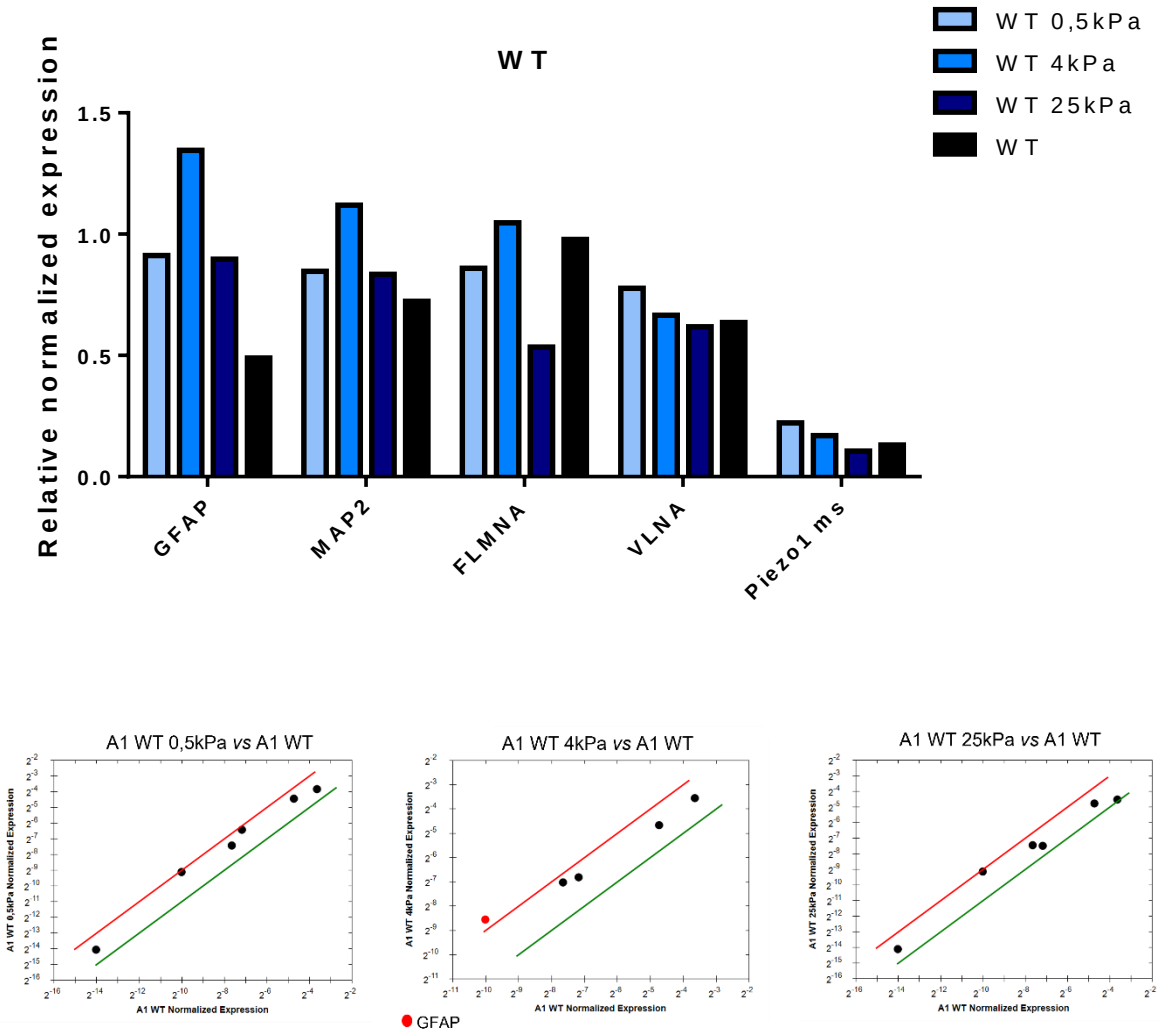

Figure 39 **mRNA expression level in WT cells plated for ten days in different substrates**. The graphs below showed the expression differences calculate in the range two-fold changes normalized on A1 WT plated on plasticware. Diagrams express the relative gene expression level compared to the internal standard GAPDH and H3.

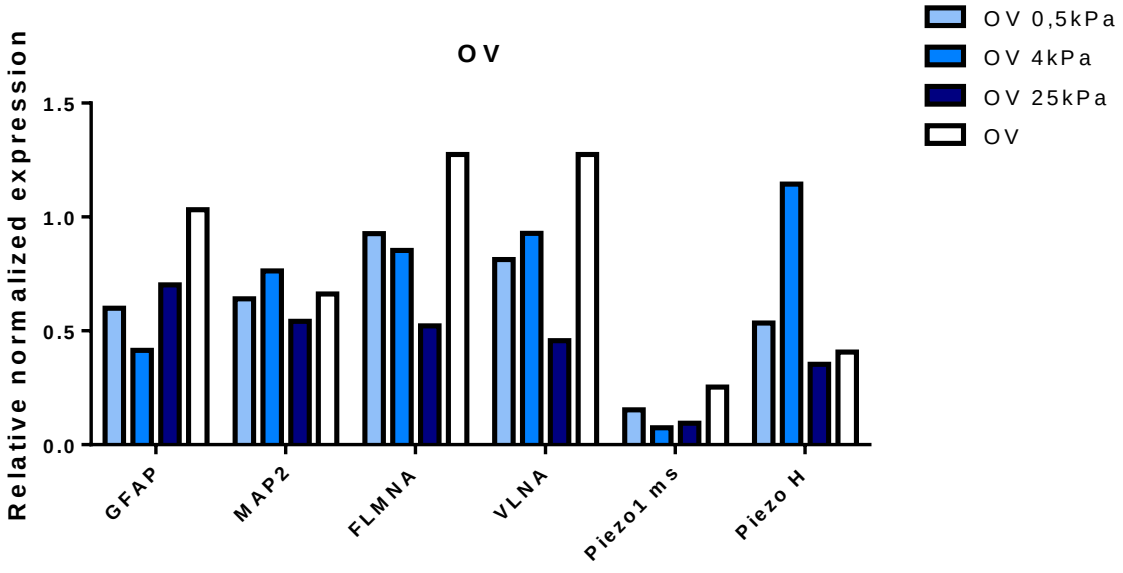

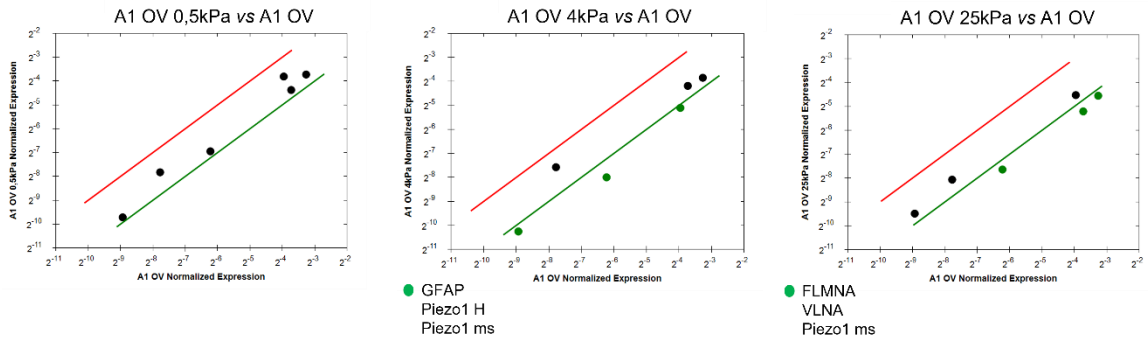

Figure 40 **mRNA expression level in A1 OV cells plated for ten days in different substrates**. The graphs below showed the expression differences calculate in the range of two-fold changes normalized on A1 OV plated on plasticware. Diagrams express the relative gene expression level compared to the internal standard GAPDH and H3**.**

5.4 AMYLOID-BETA$_{1-42}$

Another major aim of this study is to find a link between amyloid-beta peptides and the activity Piezo1 channel in order to add a new piece of knowledge to the complicated pathogenesis of AD. In collaboration with Prof. Claudio Canale, we optimized an elution protocol (lyophilisation followed by dissolution in PBS) to obtain monomeric peptide Aβ_{1-42} and performed Atomic Force Microscopy (AFM) imaging to estimate the time-course of Aβ_{1-42} aggregation. AFM images display that at tome 0 or up to 5 hours after dissolution Aβ_{1-42} is mainly in a monomeric state; the amyloidogenic process produced aggregates after 24 hours, and fibrils after 48 (*Fig.41*).

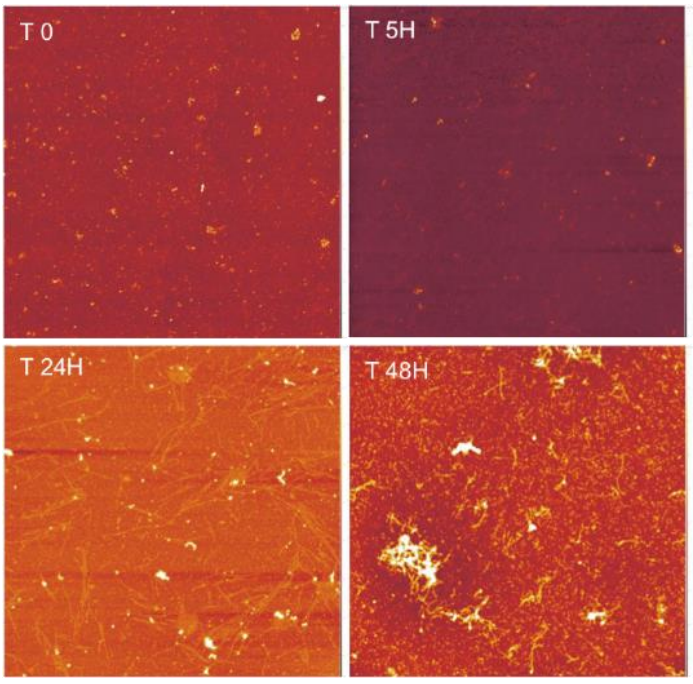

Figure 41 **Atomic Force Microscopy (AFM) imaging.** Analysis of the amyloid aggregates as assessed by Atomic Force Microscopy (AFM). AFM pictures represent a comparative view of deposited Aβ1-42 amyloid aggregates, with representative peptide (T0-T5) aggregates (T24) and fibrils (T48).

Aβ_{1-42} is known reduced cell viability, being considered a main actor in neurodegeneration in Alzheimer's patients. So, we validate the effect of Aβ_{1-42} following the elution protocol we developed, measuring cell viability using the MTT assay (*Fig.42*).

WT and OV A1 cell lines are both affected by the accumulation of $A\beta_{1-42}$. The reduction of cell viability as reported in Fig. starts after only 24h after incubation with $A\beta_{1-42}$ and increases statistically with time. The overexpression of Piezo1 does not modify $A\beta_{1-42}$ effect on A1 cells.

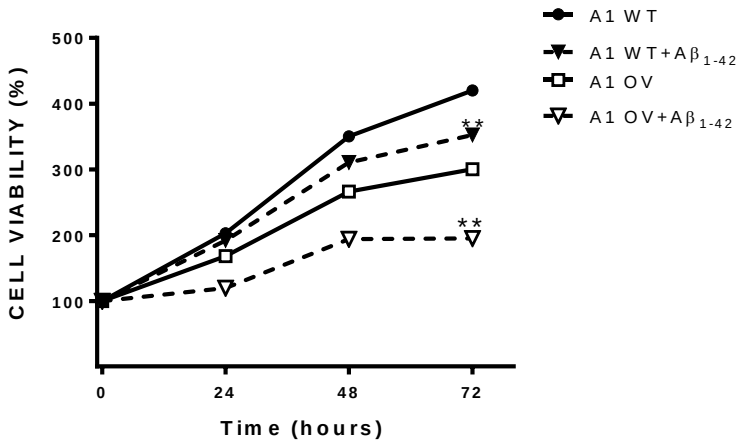

Figure 42 **$A\beta_{1-42}$ reduced cell viability of WT and OV A1 cells.** A1 WT cell viability was evaluated by MTT assay. The $A\beta_{1-42}$ was diluted in PBS to final concentration of 50µM and added after dilution in the medium at the final concentration of [1µM]. Values taken, as a percentage on time zero, are the average of two independent experiments, performed in quadruplicate (**p < 0.05 one-way ANOVA).

As previously described, according to cell types, the presence of Amyloid-beta was proposed to change the expression of Piezo1. So, through a Real-Time PCR we evaluated possible changes in the expression of the channel after Amyloid-beta [1µM] treatment. The histogram in *Fig.43* shows that the expression level of Piezo1 ms in WT and OV cell lines after 24h $A\beta_{1-42}$ treatment seem to be reduced, while after 48h go back to physiological level, but any statistical difference is revealed.

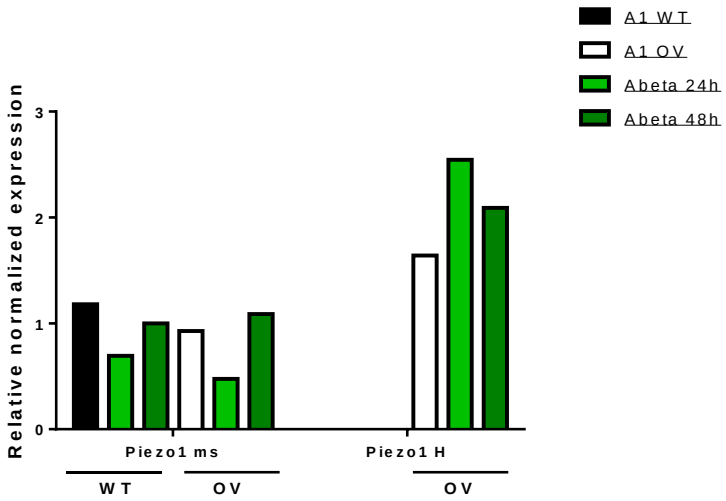

Figure 43 **Piezo1 expression level after $A\beta_{1-42}$ treatment.** Real-time PCR of Piezo1 expression after $A\beta_{1-42}$ treatment in A1 cell lines. GAPDH and H3 were used as internal standards.

Then we also performed a single-cell calcium imaging in A1 WT cell line treated with $A\beta_{1-42}$. After 24 and 48h of cell incubation with the peptide, we treated the cells with Yoda1 to monitor the effect on the activity Piezo1 channel. These preliminary results showed in *Fig.44*, demonstrate a reduction of Piezo1 response in cells treated for 24h that seems to be recovered after 48h, paralleling the response observed in Piezo1 expression.

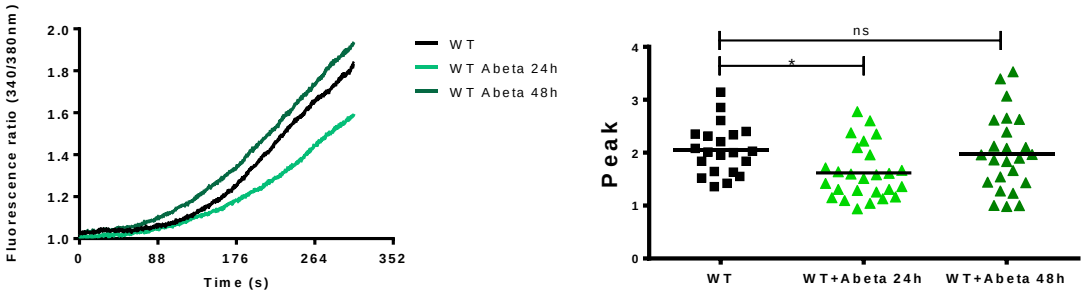

Figure 44 **Calcium imaging assay** Fura-2 ratiometric images showed changes in the cytosolic Ca^{2+} concentrations after acute YODA1 injection in A1 WT cells treated with $A\beta_{1-42}$ [1uM] after 24 or48 hours treatment (left panel). It is expressed as the medium of single-cell contributes. In the right panel, more in detail, is visible the contribution of the single cell in each experimental condition. (*<0.05 *p-value* one-way ANOVA).

The neurotoxin Gsmtx4, used as inhibitor of Piezo1 activity, is an amphipathic molecule like Amyloid-beta peptides are. This kind of molecules have been reported in previous studies[55] to be able to modulate membrane mechanics. So, from a mechanical point of

view, we evaluated whether after 24-hour treatment of A1 WT cells with amyloid-beta or Gsmtx4 changes in the elasticity of the A1 WT cells will occur. To perform this experiment, we used an upgraded version of Piuma-Chiaro in Glasgow (School of Engineering) characterized by higher sensibility. The results depicted in Fig. show that after a 24h treatment with Gsmtx4 (3 µM), elasticity of A1 WT cells was reduced. Conversely, after 24 and 48h of treatment with amyloid-beta only a slight reduction, not statistically significant, was detected. Instead, an acute insult of amyloid-beta (T0) produces a significant increase of A1 cells elasticity (*Fig.45*).

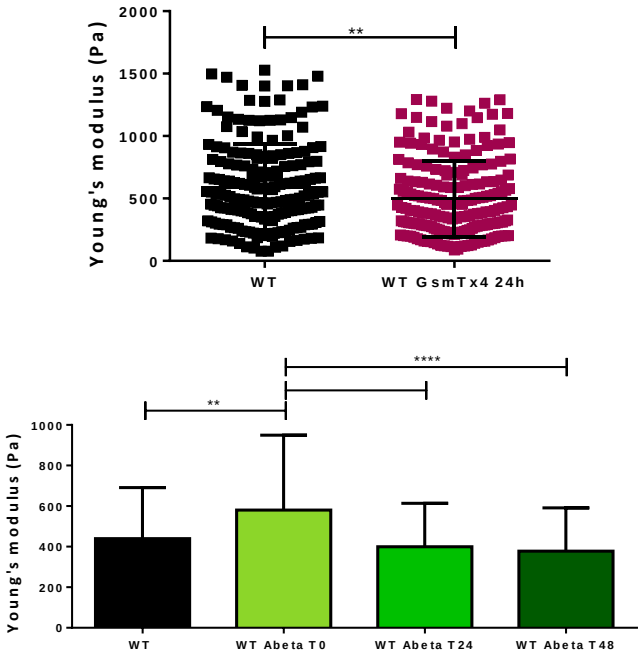

Figure 45 **Elasticity of A1 cell line.** The measures were taken with the nanoindenter CHIARO (Optics11). The upper graph shows the effect of 24h treatment with Gsmtx4 3µM. Dots represent values for individual cells. The $A\beta_{1\text{-}42}$ was diluted in PBS to a final concentration of 50µM and added after dilution in the medium at the final concentration of [1µM]. The graph below shows, the differences of the Young's modulus after the treatment with $A\beta_{1\text{-}42}$ at three different time points. (**<0.05 *p-value,* one-way ANOVA).

To confirm the possible reduction of A1 WT cells treated with amyloid-beta, YAP nuclear translocation was measured as previously described. Fig. shows a reduction in nuclear translocation of Yap.

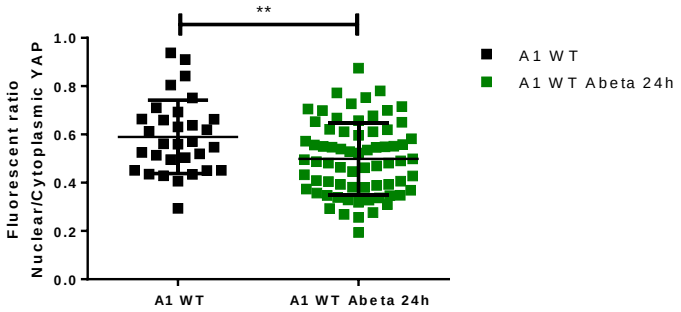

Figure 46 **Nuclear/cytoplasmatic YAP quantification** The $A\beta_{1-42}$ was diluted in PBS to a final concentration of 50µM and added after dilution in the medium at the final concentration of [1µM]. The graph represents the nuclear/cytoplasmic YAP ratios quantification by ImageJ analysis. Dots represent values for individual cells. (**<0.05 *p-value* t-student test)

6. DISCUSSION

Mechanical properties of cells are interestingly involved in several biological and pathological aspects. It is remarkable how carcinogenesis modifies several mechanical aspects of cells, including the elasticity, and how these changes are related to the increase of cancer malignancy. This to such an extent that the discrimination of mechanical property could be considered a new diagnostic tool. For this reason, new instruments and software to better measure and analyse these aspects are designed, and Piuma-CHIARO nanoindenter is one of them. One collateral project of my PhD research project, but functional to all the subsequent evaluations, was focused on the characterization of a protocol for the correct approach to nanoindentation with CHIARO.

In-vitro, cell manipulation needs an appropriate handle for each process to avoid that possible change in their properties may alter the analysed parameters. Thus, usually, the good standard provides that different cell lines or different cell characteristics should be compared at the same cell passage and in a constant percentage of confluency. Many other characteristics should be considered. So, we took care to underlie how and when cell elasticity may be affected in various *in-vitro* cell conditions. We showed that cell starvation is important to reduce the variability of data to obtain a tighter data distribution (*Fig.13*). Without serum or growth factor, it is possible to synchronize all the cells in cell cycle phase G0-G1, so it is possible to eliminate the other cycle phase (G2-M) characterized with a significant remodelling of cytoskeletal systems involved. The elasticity is a very variable parameter that changes a lot in the same sample, indeed it is necessary to take a huge number of measures to may infer something. So, we demonstrated that cellular starvation (when possible) is a useful condition to adopt.

In addition, we showed that technical replication does not affect the elasticity as biological replication does. During freezing and thawing, cells are involuntarily selected in subpopulations that may exhibit different properties. So, another possible implication is due to the passage at which the cells were frozen, which could be different. Consequently, we estimated that cell passages influence cell elasticity only when in high numbers (*Fig.16*) Cells at p20 passages are stiffer when compared to p1. Given that along cell passages there

is an increase in cell stiffness and given also that we are used primary cell culture, cell passages may be related to cell aging or senescence. These results find a relation in another work in which Kiderlen et al. demonstrated with AFM technique that senescence induced cell stiffness [56].

Depending on the percentage of cells confluency we demonstrated that cell elasticity may undergo to significant differences (*Fig.18*). A cell monolayer appears softer in comparison to isolated cells because the cellular force that occurs when cell is crowded are different and may reflect their elastic properties. Indeed, in a morphological evaluation, we showed that a cell monolayer is thicker as compared to isolated cells (*Fig.19*). So is important analyse cells in the same level of confluency but also in the same state (i.e. if they are isolated or not). Several types of cells when plated have the tendency to form islands, like glioblastoma stem cells, so to avoid experimental biases, it is important analyse all in the same condition. Another characteristic that we analysed is the cell shape because the cells are not homogenous to each other and in the same cell line is possible to identify cells with different shapes. We showed that in the cell line we analysed, two different populations in terms of shape have the same elasticity (*Fig.17*).

These considerations are meant to represent a guide for people that want to approach this kind of technique, to make them able to design an experimental plan that led to reliable results. In this respect we also used different fibroblast primary cell lines and, considering the heterogeneity of cell lines, controlling all the parameters we were able to obtain results that in absolute values are very reproducible. Importantly, to date in literature, a few of these aspects have been already addressed and analysed using other technical instruments. So, our results strongly support that the CHIARO nanoindenter is a reliable and useful tool easy to handle.

Noted the importance of cell mechanics, during my Ph.D. research activity, reported in this thesis, I tried to characterize the role of Piezo1 channel in an *in-vitro* neuron-like system to bring to light its possible implication. First of all, this cell line, A1, derived from mesencephalic progenitors, as previously described by Colucci et al., under specific experimental conditions can be differentiated in neurons endowed with GABAergic features[52]. So, we had the possibility to switch from progenitors to neurons. In response

to the differentiation process however the A1 cell line reduces the expression of Piezo1, and its fictional activity consequent to the stimulation of Yoda1 is not completely clear and adjustable. Thus, for this reason, and for the difficulty to handle A1 differentiated cells, we decided to focus our study on the most stable line, A1 WT.

Due to the evidence reported in the literature in which depletion or silencing of Piezo1 alters the cellular characteristics, worsening their functions, we evaluated how its overexpression may influence A1 morphological and functional features. The overexpression leads A1 cell line in a shape-changing, correlated to the upregulation of some cytoskeleton components genes (*Fig.28*). We also showed the upregulation of typical glial and neuronal markers (respectively GFAP and MAP2). The concomitant overexpression of both markers could be explained by the fact that we are studying neural precursors cells, so, possibly, in an initial phase of differentiation before the final commitment. But from another point of view, this upregulation may be associated with the structural cytoskeleton reorganization. Indeed, these are also considered structural proteins: Map2, which belong to a family of MAPs (microtubule-associated proteins) with the role of stabilizing dendrites microtubules in neurons; and GFAP (glial fibrillary acid protein) that intermediate filaments (IF) known as cytoskeleton structural components. Hence, this overexpression could be related more to the alteration of cell shape than to a lineage choice.

The combination of all these observations prompted us to evaluate a possible change in the elastic properties of A1 OV, and thanks to the CHIARO nanoindenter we assessed these features in the cell model in study. At odd to what was discussed before on the standardization of the indentation protocol, the starvation, as we have planned it, could not be used on these cells. Placing the A1 cells in a state of serum deprivation, as described, induces them to differentiate, then to the formation of a new cell line, with Piezo1 downregulation. Thus, in this case, using this procedure we would have introduced an extra bias. We showed a slight increase in cell stiffness in A1 OV cell (*Fig.29*). We used a developing software that allow us to analyze cell elasticity in two different ways. The first one is considering the cell as a homogenous elastic material without distinguishing the contribution of the other cellular components. The other one is able to discriminate the stiffness of the actin cortex from the bulk. Our results suggest a general increase in cell stiffness with a more specific increase in the actin cortex stiffness. The actin cortex is a layer just below the membrane, so it can influence Piezo1 activity, or Piezo1 needs to be

supported by an elevated number of cytoskeleton components recruiting them in the juxta-membrane compartment and resulting in cell stiffening.

Then A1 OV showed a reduction in viability which may be usually lined to a reduction in cells proliferation (*Fig.27*). Thus, both the enhancement of the channel activity with the use of Yoda1 stimulation (*Fig.22*) and Piezo1 overexpression leads to a common reduction in cell viability. Moreover, as we expected the overexpression leads to a more sensibilization of Piezo1, which elicits its activity after the stimulation at lower [Yoda-1] compared to WT one. But, due to the presence of a high number of channels the EC50 is lower in A1 OV because it needs more molecules to reach the maximum molecule effect.

As previously discussed, the environment in which cells are embedded is important for their physiological an pathological behaviour. It was demonstrated that different substrate stiffness can modulate the lineage choice of adult stem cells and that Piezo1 expression is important for sensing the stiffness of the environment determining the correct axon growth during brain developing or to the correct lineage choice in human neural stem cell[57],[41]. In A1 cell lines, we underlie that the substrate really affected the behaviour of the cell. We were interested to see whether the overexpression of Piezo1 could in such a way lead cells to a different response, with, for example, the mitigation of the effect that the cells undergo in distinct substrates. What we have seen, instead, is that in many aspects, which we will now describe, A1 WT cells plated in different substrates appear to be similar to A1 OV cells. The activity of Piezo1 under the stimulation of Yoda1 is higher for the substrate in the range of 4 and 25kPa, but comparable to the A1 OV response (*Fig.34*). Consequently, we demonstrated that also the initial amount of [iCa^{++}] is comparable and higher in respect WT line in plasticware (*Fig.36*). We suggest that these different behaviours could be related to a different membrane organization and tension. Indeed, cells plated on a softer substrate and A1 OV plated in plasticware have in common a decrease in cell eccentricity, the measure how the cell are approaching to be a sphere (*Fig.33*). In this condition we suggested an increase in membrane tension. It is known that membrane tension is the cause of an hyperactivation of Piezo1 which may leads to an abnormal accumulation of [iCa^{++}] and a higher response to Yoda1.

It was previously demonstrated that also a very small change in stiffness can change the behaviour of the cells [57].For that reason, we have to underlie that our data are made considering the scale of substrate stiffness from 0,5 to 25kPa, like a softer substrate in comparison with the very stiffer substrate of the common in vitro culture ($1x10^7$kPa).

In order to confirm that cellular stiffness could be related to an increased expression in cytoskeleton components, we show that A1 WT cell plated in a soft substrate does not modify the amount of these genes, and their elasticity results to be lower, but it increases in parallel with substrate stiffness (*Fig.38*).

Another aspect that we studied is how $A\beta_{1-42}$ influences the mechanics of A1 cell line. Mechanical processes involve the pathogenesis of Alzheimer's disease and Piezo1 is involved. It is overexpressed in active-astrocytes associated with amyloid plaques and downregulated in neurons[58]. Also, it seems that Piezo1 inhibition can attenuate demyelination[59]. We preliminarily demonstrated how $A\beta_{1-42}$ is able to change cell stiffness. After 24 and 48 hours when $A\beta_{1-42}$ turned into the fibrillar form the elasticity of the cell decreases compared to the WT ones. But it is more interesting the effect that showed after an acute injection that seems to lead to a cell stiffening (*Fig.45*).

It is known Piezo1 downregulation occurs in neurons in the proximity of amyloid-plaques, so we hypothesized that its overexpression may prevent the mechanical alteration due to $A\beta_{1-42}$ accumulation. So, we have preliminarily tested whether also $A\beta_{1-42}$-mediated cytotoxicity could be prevented increasing Piezo1 cell content, but on the odd, the channel overexpression did not modify $A\beta_{1-42}$ effect on A1 cells (*Fig.42*). Due to time limits, these experiments will require further validation that was not possible to perform during the Ph.D. timeframe.

7. CONCLUSIONS

A1 cells express neuronal markers and show a neuron-like behaviour; thus, they are a suitable model for pharmacological studies in neurosciences and for research concerning neurodegenerative diseases (in particular Alzheimer's disease). Furthermore, a growing body of evidence suggests that mechanical properties of neurons play a role in such pathologies and that changes in the biomechanics of the cells can induce or sustain the onset of cellular activities resulting in neurological symptoms or even neurodegeneration. Piezo1 expression and activity are important for the correct functioning of several biological aspects: both its inhibition and activation may have a potential in treating different pathologies. In reason why different cells and tissues are under the influences of different environments with various pathways and mechanical forces at play. This indicates the clear need to highlight the effects of mechanotransduction, which will represent a novel but relevant field of study in neurobiology and neuropharmacology.

PUBLICATIONS OBTAINED DURING THE Ph.D. TRAINING

1. Thellung S, Corsaro A, Bosio AG, Zambito M, Barbieri F, Mazzanti M, Florio T. 'Emerging Role of Cellular Prion Protein in the Maintenance and Expansion of Glioma Stem Cells'. Cells 2019 Nov18;8(11):1458
2. Giulio Capponi, Martina Zambito, Igor Neri, Francesco Cottone, Maurizio Mattarelli, Massimo Vassalli, Silvia Caponi and Tullio Florio 'Cellular Mechanosensitivity: Validation of an Adaptable 3D-Printed Device for Microindentation' to be submitted to Nanomaterials
3. F. Viti, F. Pramotton, M.Martufi, R. Magrassi, N. Pedemonte, F. Cella Zanacchi, M. Alampi, M. Zambito, G. Santamaria, V. Tomati , C. Giampietro, T. Florio, F. Beltrame, M. Vassalli, I. Ceccherini ՛Morpho-mechanical phenotyping of fibroblasts from patients affected with visceral myopathy' manuscript in preparation.
4. F. Viti, M. Zambito, M. Alampi, A.G. Bosio, T. Florio, M. Vassalli 'Spanning over the indentation condition' manuscript in preparation.

ABSTRACT

1. Martina Zambito, Stefano Thellung, Alessandro Corsaro, Federica Viti, Massimo Vassalli and Tullio Florio. Mechanosensitive and pharmacological properties of Piezo1 channel in embryonic mesencephalic neuron-derived cells (2nd brainstorming research assembly for young neuroscientists. Milan 14-15-16th November 2019) (POSTER PRESENTATION)
2. Martina Zambito, Stefano Thellung, Alessandro Corsaro, Federica Viti, Massimo Vassalli and Tullio Florio. Substrate's stiffness changes the behavior of immortalized mesencephalic neuron-derived cells (4th BraYn assembly for young neuroscientists) (POSTER PRESENTATION)

Meetings attendance:

- XXIII International School of Pure and Applied Biophysics "Emerging Tools in Biomechanics: from tissues down to single molecules" in Venice, 2019.
- 'Nanoengineering for Mechanobiology meeting' Camogli, Genova, Italy 24-27 March 2019
- BraYn- 2nd Brainstorming Research Assembly for Young Neuroscientists, 14th-15th -16th November 2019. Abstract:
- BraYn- 4th Brainstorming Research Assembly for Young Neuroscientists, 21th-22th-23th October 2021. Abstract:

8. BIBLIOGRAPHY

[1] D. P. Corey and A. J. Hudspeth, 'Response latency of vertebrate hair cells', *Biophys. J.*, vol. 26, no. 3, pp. 499–506, 1979, doi: 10.1016/S0006-3495(79)85267-4.

[2] O. P. Hamill and B. Martinac, 'Molecular basis of mechanotransduction in living cells', *Physiol. Rev.*, vol. 81, no. 2, pp. 685–740, 2001, doi: 10.1152/physrev.2001.81.2.685.

[3] R. Xiao and X. Z. S. Xu, 'Mechanosensitive channels: In touch with Piezo', *Curr. Biol.*, 2010, doi: 10.1016/j.cub.2010.09.053.

[4] R. Xiao and X. Z. S. Xu, 'Mechanosensitive channels: In touch with Piezo', *Curr. Biol.*, vol. 20, no. 21, 2010, doi: 10.1016/j.cub.2010.09.053.

[5] K. Satoh *et al.*, 'A novel membrane protein, encoded by the gene covering KIAA0233, is transcriptionally induced in senile plaque-associated astrocytes', *Brain Res.*, 2006, doi: 10.1016/j.brainres.2006.06.050.

[6] B. J. McHugh, R. Buttery, Y. Lad, S. Banks, C. Haslett, and T. Sethi, 'Integrin activation by Fam38A uses a novel mechanism of R-Ras targeting to the endoplasmic reticulum', *J. Cell Sci.*, 2010, doi: 10.1242/jcs.056424.

[7] B. Coste *et al.*, 'Piezo1 and Piezo2 are essential components of distinct mechanically activated cation channels', *Science (80-.).*, 2010, doi: 10.1126/science.1193270.

[8] J. Ge *et al.*, 'Architecture of the mammalian mechanosensitive Piezo1 channel', *Nature*, 2015, doi: 10.1038/nature15247.

[9] Q. Zhao *et al.*, 'Structure and mechanogating mechanism of the Piezo1 channel', *Nature*, 2018, doi: 10.1038/nature25743.

[10] J. Li *et al.*, 'Piezo1 integration of vascular architecture with physiological force', 2014, doi: 10.1038/nature13701.

[11] S. S. Ranade *et al.*, 'Piezo1, a mechanically activated ion channel, is required for vascular development in mice', doi: 10.1073/pnas.1409233111.

[12] C. Bae, R. Gnanasambandam, C. Nicolai, F. Sachs, and P. A. Gottlieb, 'Xerocytosis is caused by mutations that alter the kinetics of the mechanosensitive channel PIEZO1', *Proc. Natl. Acad. Sci. U. S. A.*, vol. 110, no. 12, 2013, doi: 10.1073/pnas.1219777110.

[13] I. Andolfo *et al.*, 'Multiple clinical forms of dehydrated hereditary stomatocytosis arise from mutations in PIEZO1', *Blood*, vol. 121, no. 19, pp. 3925–3935, 2013, doi: 10.1182/blood-2013-02-482489.

[14] S. M. Cahalan, V. Lukacs, S. S. Ranade, S. Chien, M. Bandell, and A. Patapoutian, 'Piezo1 links mechanical forces to red blood cell volume', *Elife*, vol. 4, no. MAY, pp. 1–12, 2015, doi: 10.7554/eLife.07370.

[15] E. Fotiou *et al.*, 'Novel mutations in PIEZO1 cause an autosomal recessive generalized lymphatic dysplasia with non-immune hydrops fetalis', *Nat. Commun.*,

vol. 6, pp. 1–6, 2015, doi: 10.1038/ncomms9085.

[16] V. Lukacs *et al.*, 'Impaired PIEZO1 function in patients with a novel autosomal recessive congenital lymphatic dysplasia', *Nat. Commun.*, vol. 6, pp. 1–7, 2015, doi: 10.1038/ncomms9329.

[17] K. Retailleau *et al.*, 'Piezo1 in Smooth Muscle Cells Is Involved in Hypertension-Dependent Arterial Remodeling', *Cell Rep.*, vol. 13, no. 6, pp. 1161–1171, 2015, doi: 10.1016/j.celrep.2015.09.072.

[18] J. Liang *et al.*, 'Stretch-activated channel Piezo1 is up-regulated in failure heart and cardiomyocyte stimulated by Angii', *Am. J. Transl. Res.*, vol. 9, no. 6, pp. 2945–2955, 2017.

[19] W. Lee *et al.*, 'Synergy between Piezo1 and Piezo2 channels confers high-strain mechanosensitivity to articular cartilage', *Proc. Natl. Acad. Sci.*, 2014, doi: 10.1073/pnas.1414298111.

[20] B. J. McHugh, A. Murdoch, C. Haslett, and T. Sethi, 'Loss of the integrin-activating transmembrane protein Fam38A (Piezo1) promotes a switch to a reduced integrin-dependent mode of cell migration', *PLoS One*, vol. 7, no. 7, 2012, doi: 10.1371/journal.pone.0040346.

[21] C. Alibert, B. Goud, and J. B. Manneville, 'Are cancer cells really softer than normal cells?', *Biol. Cell*, vol. 109, no. 5, pp. 167–189, 2017, doi: 10.1111/boc.201600078.

[22] J. Wu, A. H. Lewis, and J. Grandl, 'Touch, Tension, and Transduction – The Function and Regulation of Piezo Ion Channels', *Trends Biochem. Sci.*, vol. 42, no. 1, pp. 57–71, Jan. 2017, doi: 10.1016/j.tibs.2016.09.004.

[23] X. Chen *et al.*, 'A Feedforward Mechanism Mediated by Mechanosensitive Ion Channel PIEZO1 and Tissue Mechanics Promotes Glioma Aggression', *Neuron*, 2018, doi: 10.1016/j.neuron.2018.09.046.

[24] T. Zhang, S. Chi, F. Jiang, Q. Zhao, and B. Xiao, 'A protein interaction mechanism for suppressing the mechanosensitive Piezo channels', *Nat. Commun.*, 2017, doi: 10.1038/s41467-017-01712-z.

[25] K. Poole, R. Herget, L. Lapatsina, H. D. Ngo, and G. R. Lewin, 'Tuning Piezo ion channels to detect molecular-scale movements relevant for fine touch', *Nat. Commun.*, vol. 5, 2014, doi: 10.1038/ncomms4520.

[26] C. Wetzel *et al.*, 'A stomatin-domain protein essential for touch sensation in the mouse', *Nature*, vol. 445, no. 7124, pp. 206–209, 2007, doi: 10.1038/nature05394.

[27] Y. Qi, L. Andolfi, F. Frattini, F. Mayer, M. Lazzarino, and J. Hu, 'Membrane stiffening by STOML3 facilitates mechanosensation in sensory neurons', *Nat. Commun.*, vol. 6, 2015, doi: 10.1038/ncomms9512.

[28] I. Borbiro, D. Badheka, and T. Rohacs, 'Activation of TRPV1 channels inhibits mechanosensitive piezo channel activity by depleting membrane phosphoinositides', *Sci. Signal.*, 2015, doi: 10.1126/scisignal.2005667.

[29] K. Retailleau *et al.*, 'Piezo1 in Smooth Muscle Cells Is Involved in Hypertension-Dependent Arterial Remodeling', *Cell Rep.*, 2015, doi: 10.1016/j.celrep.2015.09.072.

[30] T. M. Suchyna *et al.*, 'Identification of a peptide toxin from Grammostola spatulata spider venom that blocks cation-selective stretch-activated channels', *J. Gen. Physiol.*, vol. 115, no. 5, pp. 583–598, 2000, doi: 10.1085/jgp.115.5.583.

[31] K. Nishizawa, M. Nishizawa, R. Gnanasambandam, F. Sachs, S. I. Sukharev, and T. M. Suchyna, 'Effects of Lys to Glu mutations in GsMTx4 on membrane binding,

peptide orientation, and self-association propensity, as analyzed by molecular dynamics simulations', *Biochim. Biophys. Acta - Biomembr.*, vol. 1848, no. 11, pp. 2767–2778, 2015, doi: 10.1016/j.bbamem.2015.09.003.

[32] R. Gnanasambandam *et al.*, 'GsMTx4: Mechanism of Inhibiting Mechanosensitive Ion Channels', *Biophys. J.*, vol. 112, no. 1, pp. 31–45, 2017, doi: 10.1016/j.bpj.2016.11.013.

[33] R. Syeda *et al.*, 'Chemical activation of the mechanotransduction channel Piezo1', *Elife*, vol. 4, no. MAY, 2015, doi: 10.7554/eLife.07369.

[34] E. L. Evans *et al.*, 'Yoda1 analogue (Dooku1) which antagonizes Yoda1-evoked activation of Piezo1 and aortic relaxation', *Br. J. Pharmacol.*, vol. 175, no. 10, pp. 1744–1759, 2018, doi: 10.1111/bph.14188.

[35] Y. Wang *et al.*, 'A lever-like transduction pathway for long-distance chemical- and mechano-gating of the mechanosensitive Piezo1 channel', *Nat. Commun.*, vol. 9, no. 1, 2018, doi: 10.1038/s41467-018-03570-9.

[36] D. A. Fletcher and R. Dyche Mullins, 'Cell mechanics and the cytoskeleton REVIEW INSIGHT', doi: 10.1038/nature08908.

[37] B. Geiger, J. P. Spatz, and A. D. Bershadsky, 'Environmental sensing through focal adhesions', *Nat. Rev. Mol. Cell Biol.*, vol. 10, no. 1, pp. 21–33, 2009, doi: 10.1038/nrm2593.

[38] H. Mohammadi and C. A. McCulloch, 'Impact of elastic and inelastic substrate behaviors on mechanosensation', *Soft Matter*, vol. 10, no. 3, pp. 408–420, 2014, doi: 10.1039/c3sm52729h.

[39] A. J. Engler, S. Sen, H. L. Sweeney, and D. E. Discher, 'Matrix Elasticity Directs Stem Cell Lineage Specification', *Cell*, vol. 126, no. 4, pp. 677–689, 2006, doi: 10.1016/j.cell.2006.06.044.

[40] S. Dupont *et al.*, 'Role of YAP/TAZ in mechanotransduction', *Nature*, vol. 474, no. 7350, pp. 179–184, 2011, doi: 10.1038/nature10137.

[41] M. M. Pathak *et al.*, 'Stretch-activated ion channel Piezo1 directs lineage choice in human neural stem cells', *Proc. Natl. Acad. Sci.*, 2014, doi: 10.1073/pnas.1409802111.

[42] X. Cai, K. C. Wang, and Z. Meng, 'Mechanoregulation of YAP and TAZ in Cellular Homeostasis and Disease Progression', *Front. Cell Dev. Biol.*, vol. 9, no. May, pp. 1–12, 2021, doi: 10.3389/fcell.2021.673599.

[43] M. Unal *et al.*, 'Micro and Nano-Scale Technologies for Cell Mechanics', *Nanobiomedicine*, vol. 1, no. October, 2014, doi: 10.5772/59379.

[44] S. Siechen, S. Yang, A. Chiba, and T. Saif, 'Mechanical tension contributes to clustering of neurotransmitter vesicles at presynaptic terminals', *Proc. Natl. Acad. Sci. U. S. A.*, vol. 106, no. 31, pp. 12611–12616, 2009, doi: 10.1073/pnas.0901867106.

[45] I. Tasaki, K. Kusano, and P. M. Byrne, 'Rapid mechanical and thermal changes in the garfish olfactory nerve associated with a propagated impulse', *Biophys. J.*, vol. 55, no. 6, pp. 1033–1040, 1989, doi: 10.1016/S0006-3495(89)82902-9.

[46] G. Landouré *et al.*, 'Mutations in TRPV4 cause Charcot-Marie-Tooth disease type 2C', 2009, doi: 10.1038/ng.512.

[47] G. Zü and G. Reiser, 'Calcium Dysregulation and Homeostasis of Neural Calcium in the Molecular Mechanisms of Neurodegenerative Diseases Provide Multiple Targets for Neuroprotection', Accessed: Dec. 16, 2021. [Online]. Available:

www.liebertonline.com=ars.

[48] M. C. Murphy *et al.*, 'Regional brain stiffness changes across the Alzheimer's disease spectrum', *NeuroImage Clin.*, 2016, doi: 10.1016/j.nicl.2015.12.007.

[49] M. Velasco-Estevez *et al.*, 'Infection augments expression of mechanosensing Piezo1 channels in amyloid plaque-reactive astrocytes', *Front. Aging Neurosci.*, 2018, doi: 10.3389/fnagi.2018.00332.

[50] A. A. Ungureanu *et al.*, 'Amyloid beta oligomers induce neuronal elasticity changes in age-dependent manner: A force spectroscopy study on living hippocampal neurons', *Sci. Rep.*, vol. 6, no. May, pp. 1–13, 2016, doi: 10.1038/srep25841.

[51] D. Drabik, G. Chodaczek, and S. Kraszewski, 'Effect of amyloid-β monomers on lipid membrane mechanical parameters–potential implications for mechanically driven neurodegeneration in alzheimer's disease', *Int. J. Mol. Sci.*, vol. 22, no. 1, pp. 1–12, 2021, doi: 10.3390/ijms22010018.

[52] G. L. Colucci-D'Amato, A. Tino, R. Pernas-Alonso, J. M. H. Ffrench-Mullen, and U. Di Porzio, 'Neuronal and glial properties coexist in a novel mouse CNS immortalized cell line', *Exp. Cell Res.*, 1999, doi: 10.1006/excr.1999.4636.

[53] D. Chavan *et al.*, 'Ferrule-top nanoindenter: An optomechanical fiber sensor for nanoindentation', *Rev. Sci. Instrum.*, vol. 83, no. 11, 2012, doi: 10.1063/1.4766959.

[54] I. Lüchtefeld *et al.*, 'Elasticity spectra as a tool to investigate actin cortex mechanics', *J. Nanobiotechnology*, vol. 18, no. 1, pp. 1–11, 2020, doi: 10.1186/s12951-020-00706-2.

[55] M. M. Maneshi, L. Ziegler, F. Sachs, S. Z. Hua, and P. A. Gottlieb, 'Enantiomeric Aβ peptides inhibit the fluid shear stress response of PIEZO1', *Sci. Rep.*, 2018, doi: 10.1038/s41598-018-32572-2.

[56] S. Kiderlen, C. Polzer, J. O. Rädler, D. Docheva, H. Clausen-Schaumann, and S. Sudhop, 'Age related changes in cell stiffness of tendon stem/progenitor cells and a rejuvenating effect of ROCK-inhibition', *Biochem. Biophys. Res. Commun.*, vol. 509, no. 3, pp. 839–844, 2019, doi: 10.1016/j.bbrc.2019.01.027.

[57] D. E. Koser *et al.*, 'Mechanosensing is critical for axon growth in the developing brain', *Nat. Neurosci.*, 2016, doi: 10.1038/nn.4394.

[58] M. Velasco-Estevez, S. O. Rolle, M. Mampay, K. K. Dev, and G. K. Sheridan, 'Piezo1 regulates calcium oscillations and cytokine release from astrocytes', *Glia*, vol. 68, no. 1, pp. 145–160, 2020, doi: 10.1002/glia.23709.

[59] M. Velasco-Estevez, K. K. E. Gadalla, N. Liñan-Barba, S. Cobb, K. K. Dev, and G. K. Sheridan, 'Inhibition of Piezo1 attenuates demyelination in the central nervous system', *Glia*, vol. 68, no. 2, pp. 356–375, 2020, doi: 10.1002/glia.23722.